Spring 2019

Build strategy investigation of TI-6AL-4V produced via a hybrid additive manufacturing process

Lei Yan

Department: Mechanical and Aerospace Engineering

BUILD STRATEGY INVESTIGATION OF TI-6AL-4V PRODUCED VIA A HYBRID ADDITIVE MANUFACTURING PROCESS

by

LEI YAN

A DISSERTATION

Presented to the Faculty of the Graduate School of the

MISSOURI UNIVERSITY OF SCIENCE AND TECHNOLOGY

In Partial Fulfillment of the Requirements for the Degree

DOCTOR OF PHILOSOPHY

in

MECHANICAL ENGINEERING

2019

Approved
Dr. Frank Liou, Advisor
Dr. K. Chandrashekhara
Dr. Heng Pan
Dr. Joseph W. Newkirk
Dr. Caizhi Zhou

PUBLICATION DISSERTATION OPTION

This dissertation consists of the following three articles that have been published or submitted for publication as follows:

Paper I, pages 7-26 have been published in JOM.

Paper II, pages 27-38 have been published in Manufacturing Letters.

Paper III, pages 39-52 have been published in The 29th Annual International Solid Freeform Fabrication Symposium.

ABSTRACT

Till now, laser metal deposition (LMD) has been developed with the capability of near-net shape high-performance metal parts fabrication, especially complicated titanium alloys, nickel alloys, and aluminum alloys. However, LMD processed parts usually do not meet end-use requirements without post treatments. In-process part quality inspection and inner features machining are impossible within a single LMD process. Hybrid additive manufacturing (HAM), which integrates additive and subtractive manufacturing in one process, has been proposed to increase the feasibility of complex parts fabrication. This dissertation aims to improve the applications of Ti-6Al-4V parts fabricated via a HAM technique. The first research topic is to investigate the build strategy using the HAM process of correlating yield strength of final parts to processing parameters from both additive and subtractive processes for Ti-6Al-4V structures. The second research topic focuses on coolant residue cleaning methods, where effective cleaning methods have been generated on both oil- and water-based coolant. To reduce trial-and-error efforts and optimize large-scale parts fabrication using HAM, thermal control has become an essential factor that directly relates to the final distortion and residual stress. Hence, the third research topic is conducted on the fast prediction of thermal history in large-scale parts fabrication via a HAM process. This dissertation leads to new knowledge for the effective fabrication of metallic components via a HAM process. Moreover, the research results of the dissertation could benefit a wide range of industries.

ACKNOWLEDGMENTS

I would like to thank my Mom and Dad for their love and unconditional support in all my life.

Thanks to Dr. Frank Liou, my advisor, for encouraging me to pursue my Ph.D. and for providing ever positive support and excellent guidance. In addition, I'd like to thank Dr. Joseph Newkirk, Dr. Caizhi Zhou, Dr. Heng Pan and Dr. KC for their constructive suggestions on my work during my Ph.D. study.

I would also like to thank my (past) lab mates Xueyang, Zhiqiang, Yunlu, Wei, Xinchang, Todd, Sreekar, Aaron, Wenyuan, Yitao, and Tan for always providing generous help and making the lab environment an interesting place to work.

Last, but not least, I am grateful for my wife, Sai, and our unborn kids, whom I love more than anything. Starting a family with my beloved ones far surpasses any possible professional achievement.

TABLE OF CONTENTS

LIST OF ILLUSTRATIONS

Page

SECTION

PAPER I

PAPER II

PAPER III

LIST OF TABLES

Page

SECTION

1. INTRODUCTION

1.1. BACKGROUND

Hybrid additive manufacturing (HAM) is a relatively new process that combines the freedom of additive manufacturing with the precision of computer numerical control (CNC) to enable done-in-one ability. The interchangeability of machine heads allows in-process material adding, material removal, and quality inspection, and provides solutions for features that are difficult to machine with conventional methods, like the inner channels of an engine manifold. Different HAM systems have been investigated in recent years such as laser welding with a 5-axis milling center [1], 6-axis machining centers with diverse additive manufacturing processes [2], and MIG/MAG welding integrated with a face milling process [3]. Some HAM systems have been commercialized, such as Mazak's INTEGREX i-400 and DMG Mori's Lasertec hybrid machines. But till now, most of the reported research efforts that have been put into the HAM process are focused on hardware development and system motion control optimization, with only a few focused on the understanding of the HAM process itself, like the correlation between process window and performance of the final part.

As machining has been introduced and combined with the laser metal deposition (LMD) process, coolant has inevitably been included in the consideration of safety, cost, and machining performance of the HAM process, especially for Ti-6Al-4V parts fabrication. The coolant residue from the machining process on the machined surface,

where there will be subsequent deposits, is a potential concern for contamination and bonding strength. Although feasibility research with dry machining on additively manufactured Ti-6Al-4V parts has been performed [4], the low feed rate to achieve the same surface integrity with coolant applied is not suitable because of industrial production. Oil- and water-based coolant are the most common coolant types in Ti-6Al-4V machining [5-6]. Acetone was considered for an oil-based coolant residue removal method for its good degreasing ability and quick evaporation, but it was eliminated from consideration since the cleaning process is performed in the HM machine and the acetone will dry out or damage the system's seals. It is critical to find an appropriate coolant residue cleaning method that maintains the final part's mechanical performance and improves efficiency in production.

Large, complex, high-performance metal components are usually quite costly, even with the HAM process, compared to conventional methods. Thus, it is vital to reduce trial-and-error and plan the feasible process window in advance. To do so, a better understanding of thermal cycles during the HAM process is essential. Much efforts has been put into the temperature field analysis and is mainly based on the finite element analysis (FEA) method [7-11]. A common method used to mimic the material addition process is called the "dummy material method" [9] or the "element birth and death method" [11], which uses active elements in the finite element model according to a predefined deposition strategy. The aforementioned methods usually include a computational intensive model, as not only do the minimum required time increments in transient heat transfer analysis need to be met, but also a mesh convergence needs to be achieved, which requires a minimum element size relative to the laser beam diameter [11]. When applied,

the conventional methods used to predict transient temperature history in a large-scale part fabrication process increase the model size tremendously. In some cases, a precise description of the thermal history in the laser deposition process is not necessary and only a fast prediction of the peak temperature will be needed for the process plan. Hence, the fast prediction of thermal history for large-scale parts fabrication via the HAM process has become urgent.

Herein, to solve the aforementioned problems, this dissertation investigates the following key research topics and will benefit the guideline generation in the fabrication of large-scale, complex, high-performance metal components via the HAM process.

1.2. RESEARCH OBJECTIVES

The main objective of this research is to investigate the key technologies for improving the manufacturability of large-scale metal components using the HAM process. Three research topics are studied in depth to achieve the overall objective.

The first research topic is to correlate the process window of the HAM process with the performance of the as-built deposits. The main challenge is to figure out the significant processing parameters that affect final parts' mechanical properties and fit them into a regression model, such as the relation between processing parameters and yield strength (YS). A design of experiments (DOE) approach is proposed, for the fabrication of Ti-6Al-4V thin-wall structures, to help understand and correlate multiple HAM processing parameters with the final part's microstructure, and determining the significant factors for the yield strength (YS). Vickers hardness tests along the build height direction will also be conducted to study with the microstructure distribution within the deposit. Finite element

analysis (FEA) will be utilized to predict transient thermal history during the HAM process to help in understanding the microstructure characterization results. Based on these analyses, a strategy for planning a components fabrication via the HAM process can be obtained.

The second research topic is focused on coolant residue cleaning of the machined surface where subsequent deposition will be applied. The main goal is to effectively remove coolant residue based on the existing hardware of the HAM system without involving additional efforts. Laser rastering and compressed air embedded in the HAM machine are considered for coolant residue cleaning. The feasibility of those two methods is tested by analyzing both oil- and water-based coolant in four scenarios, where different combinations of laser heating and compressed air for coolant residue cleaning are implemented. Deposits built within the four scenarios are compared with samples deposited on dry machined surfaces by evaluating Vickers hardness and tensile test results. The outcomes will be critical for providing guidelines for HAM process production improvement.

The third research topic aims to improve fast prediction of transient thermal history in large-scale parts fabrication. The main obstacles for fast prediction with conventional methods using the FEA method lie in tremendous model size when dealing with a large-scale part simulation, which leads to lower time efficiency. Herein, two methods called track-heat-source and layer-heat-source are proposed for fast prediction of transient thermal history in large-scale part fabrication via the LMD process. The conclusions will benefit processing parameter optimization, reduce trial-and-error, and improve cost efficiency.

The outcomes of the above research topics are expected to advance the knowledge of using the HAM process in metal components fabrication. The technical developments may benefit not only the area of new component fabrication, but also other areas such as existing part modification, part repair engineering, and FEA model developing.

1.3. ORGANIZATION OF DISSERTATION

In this dissertation, three major types of research are presented and organized, as shown in Figure 1.1. Three papers have been published in accordance with those three types of research, which belong to the same core topic of strategy investigation of large-scale Ti-6Al-4V part fabrication via the HAM process.

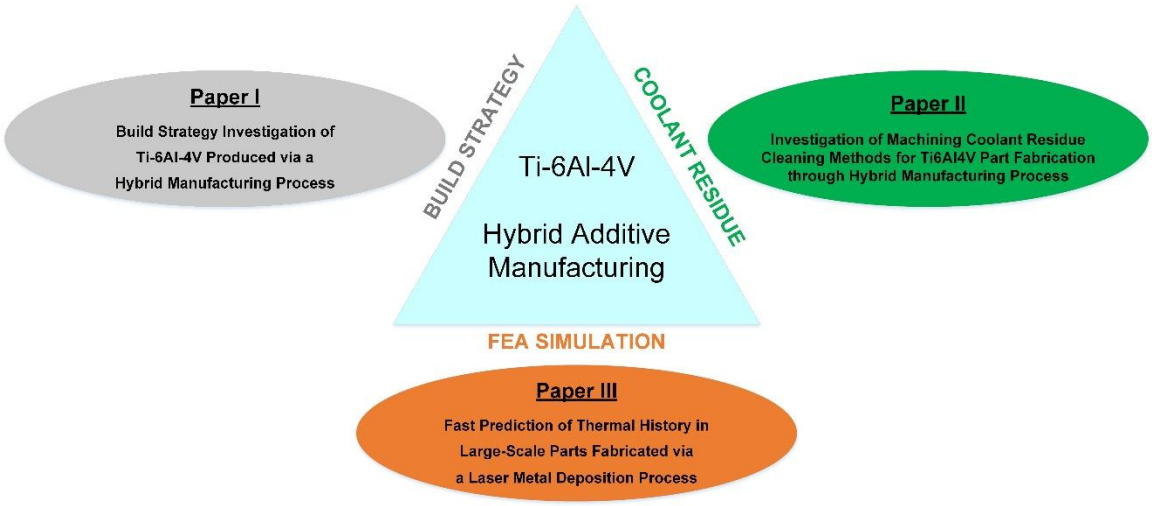

Figure 1.1. The framework of this dissertation

Paper I focuses on the correlation of processing parameters with the performance of the final deposits. This paper demonstrates the theories, methodologies, and implementation of the HAM process. It reveals the key factors for the final component's

YS, microstructure, and Vickers hardness, which can be helpful for strengthening process control and optimizing fabrication processes. Paper II emphasizes coolant residue removal in the HAM process. It provides effective procedures for both oil- and water-based coolant residue removal and helps in stability control of the HAM process and its production improvement. Paper III presents two innovative FEA models for the fast prediction of the transient thermal history in HAM process. It provides new ideas in the HAM processing parameters optimization and improvements in both cost and time efficiency.

PAPER

I. BUILD STRATEGY INVESTIGATION OF TI-6AL-4V PRODUCED VIA A HYBRID MANUFACTURING PROCESS

Lei Yan[1], Wenyuan Cui[1], Joseph W. Newkirk[2], Frank Liou[1],
Eric E. Thomas[3], Andrew H. Baker[3], James B. Castle[3]

[1]Department of Mechanical and Aerospace Engineering,
Missouri University of Science and Technology, Rolla, MO 65409
[2]Department of Materials Science and Engineering,
Missouri University of Science and Technology, Rolla, MO 65409
[3]The Boeing Company, St. Louis, MO 63043

ABSTRACT

Hybrid manufacturing (HM), which integrates additive and subtractive manufacturing in one system, has become a popular choice for near net shape fabrication of complex parts. Although the HM systems have been investigated for decades with major effort on hardware and motion control system development, less work has been done in the exploration of relationships between microstructure evolution and the HM processing parameters. Here, Ti-6Al-4V thin-wall structures are fabricated according to a design of experiments (DOE) matrix that includes four main HM processing parameters: layer height, powder feed rate, input energy density, and preheat condition. Optical microscopy is used to characterize the microstructure and relate it to the final part mechanical properties using

Vickers hardness test and tensile test. Finite element analysis (FEA) is applied to predict transient temperature history in the HM process and to help understand the microstructure type formation.

Keywords: Hybrid Manufacturing; Ti-6Al-4V; Design of Experiment; Finite Element Analysis

1. INTRODUCTION

Hybrid manufacturing (HM) is a relatively new process which combines the freedom of additive manufacturing with the precision of computer numerical control (CNC) to enable done-in-one ability. The interchangeability of machine heads allows in-process material adding, material removal, quality inspection, and provides solutions for difficult machining features with conventional methods, like inner channels of an engine manifold. Different HM systems have been investigated in recent years such as laser welding with a 5-axis milling center [1], 6-axis machining centers with diverse additive manufacturing processes [2], and MIG/MAG welding integrated with a face milling process [3]. Some HM systems have been commercialized such as Mazak's INTEGREX i-400 and DMG Mori's Lasertec hybrid machines. To the best of our knowledge, efforts put on the HM processes have mainly focused on hardware development and system motion control optimization, with less research activity on the exploration of the relationships between HM processing parameters and the resultant microstructure of the manufactured component. Herein, laser metal deposition (LMD), a blown powder additive manufacturing process, was combined with CNC milling to fabricate Ti-6Al-4V thin-wall structures. A design of experiments (DOE) approach was used to relate multiple HM processing

parameters with the final part's microstructure and determine the significant factors for the yield strength (YS). Vickers hardness tests along the build height direction were conducted to compare the microstructure distribution within the deposit. Finite element analysis (FEA) was utilized to predict transient thermal history during the HM process to help understand the microstructure characterization results.

2. MATERIALS AND METHODS

Ti-6Al-4V thin-wall structures were fabricated with two separate systems, LMD and milling, in a manner to mimic the build process of an integrated HM system. The deposition process was conducted in an in-house LMD system as shown in Figure 1a, where gas atomized Ti-6Al-4V powders (Advanced Specialty Metals, NH, USA) with -60+120 mesh size were fed through a vertical alumina tube and introduced into the melt pool. The heat source for the LMD system is a 1 kW Nd-YAG laser and deposited with a 2 mm beam diameter. In this LMD system, the laser position was fixed and the deposition was conducted by controlling the movement of the substrate. The substrates for deposition were grade 5 Ti-6Al-4V plates with dimensions 75 mm x 25 mm x 7 mm. Open-source software "LinuxCNC" was used for motion control of a 3-axis work table where the substrates were clamped. The machining system was a PCNC 1100 CNC mill with a .5" Iscar insert cutter. The modification of standard machining recipe for Ti-6Al-4V was required because of the differences in machining characteristics between LMD Ti-6Al-4V and wrought Ti-6Al-4V. Based on trial and error, the final cutting parameters were set to 450 sfm and .0027 chip per tooth using Hocut 795B cutting fluid.

To guarantee the alignment after the transfer between the LMD and the machining system, two sets of fixture were designed. The fixture designed for the LMD process is shown in Figure 1b, where three pins and a toggle clamp guaranteed the deposit at the same location related to the system coordinate frame before and after being taken out of the LMD system. The machining fixture is shown in Figure 1c, where the same working principle as the fixture of the LMD system was applied and fulfilled by two pins and two nuts.

The working principle of the HM system is depicted in Figure 1d, where machining was introduced between each LMD process and the top surface was machined to the required height and prepared for the next deposition. There are multiple processing parameters that potentially impact the evolution of microstructure in the HM process. Energy density and the layer height represents the energy input and the thermal mass within the LMD process and directly relates to the temperature and cooling rate, which are primary drivers of the microstructure type and feature size. The thermal mass accumulated in the LMD process is based on the powder introduced into the melt pool and accordingly relates to the powder feed rate. Preheating is also a factor which effects powder capture efficiency and microstructure evolution [4].

Build strategies employ different combinations of parameters in the building of a part. A DOE screening was implemented to investigate the processing parameters' impact on the resulting microstructure and Vickers hardness of the deposits. The DOE was bounded with high- and low-level values of parameters that resulted in macroscopically sound builds. These four factors are layer height, energy density, powder feed rate, and preheating condition. The selection of these bounding parameters is described below.

The laser energy density (LED) defined here is written as LED=p/v, where p is laser power (W) and v is laser transverse speed (mm/min). To save the effort of trial and error on the searching of the minimum LED value, latent heat L and $Q=m*\Delta T*C_p$ was used for the first assumption, where m denotes mass of the melted powders, ΔT is the powder temperature change from ambient temperature 300 K to its liquidus temperature of 1933 K, and is the specific heat capacity. The thickness of the final thin-wall structure was designed to 2 mm and the as-deposit structure was planned to be 3 to 3.5 mm thick.

The exploration of a suitable single track height and laser transverse speed that yielded a stable buildup with good powder capture efficiency was conducted on the in-house LMD system. A 0.5 mm single track height and 216 mm/min laser transverse speed proved sufficient and was selected. The energy efficiency of the LMD process with YAG laser is reported to be around 10% to 20% of the raw power [5]. Based on this consideration, the minimum LED needed to fabricate a 0.5 mm high and 3.5 mm wide thin-wall structure is 1.38 W/(mm/min), which corresponds to 298 W for laser power. A systematic search for a suitable range of the LED was conducted starting from 1.38 W/(mm/min), with a suitable range being obtained between 1.6 to 1.7 W/(mm/min). Optical microscopy images of the deposit's cross-sections revealed no porosity and lack of fusion, and assured full density parts. The avoidance of severe overheating was evaluated based on visual observation of deposit color, which reflected the temperature in the deposition process.

The powder feeder mass flow rate calibration results are shown in Figure 1e, where the x-axis denotes the percentage of the full feeding speed and the y-axis denotes the actual powder weight gathered at each selected speed within a minute. The experimental data was polynomial fitted with an R2 (adj.) of 0.99696. A suitable range 1.45 g/min and 1.96 g/min

was selected to fabricate 3.5-mm-thick thin-wall structures and avoid the severe issue of powder sintering on surfaces. For layer height, 4 mm and 6 mm were selected as the low and high levels. The two height values are repeatable and have enough height difference for small-scale model analysis with the DOE matrix. The preheat impact was tested under a binary scenario of no preheat and preheat, where preheat was conducted by a 200 W laser scan at 216 mm/min along the deposition path twice and the peak temperature was predicted around 1500 K with a 3D FEA model [6]. The final dimensions of the thin-wall structures were 20 mm x 2 mm x 12 mm.

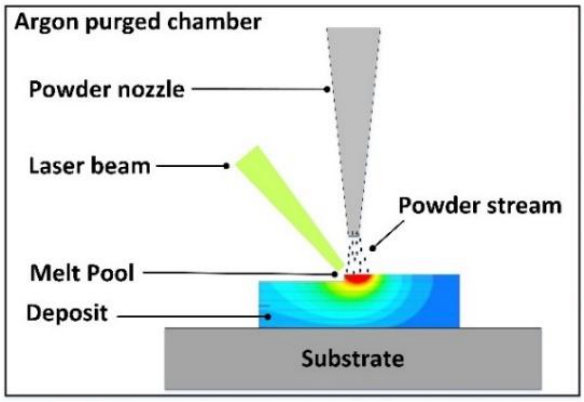

(a) schematic of the LMD process

(b) fixture for the LMD process

Figure 1. Experimental set-up

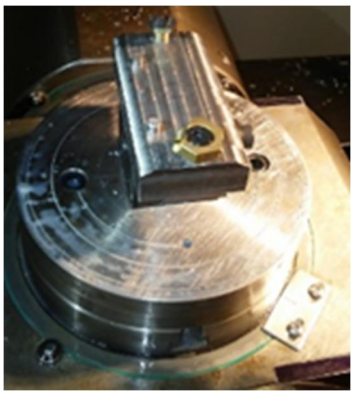

(c) fixture for the milling process

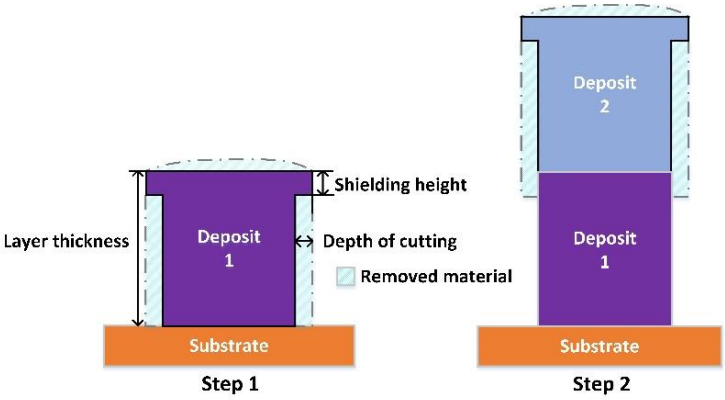

(d) schematic of the HM process

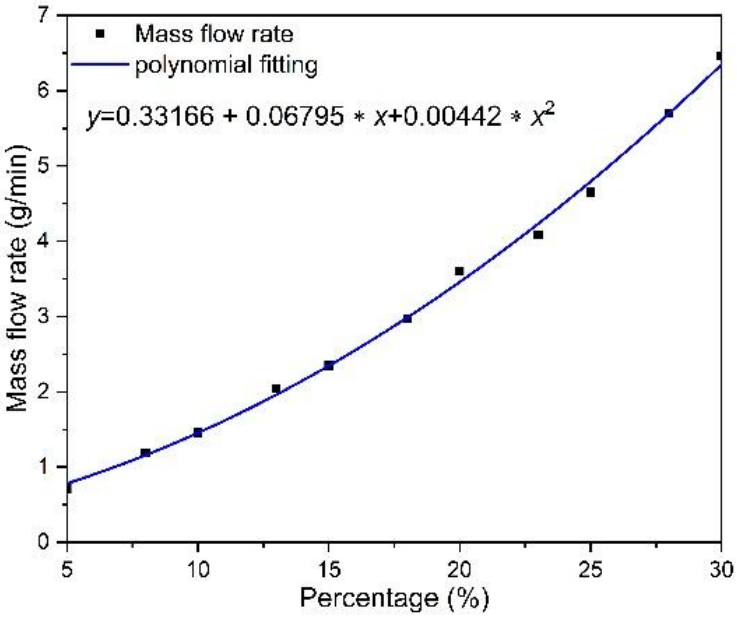

(e) powder feed rate calibration results

Figure 1. Experimental set-up (cont.)

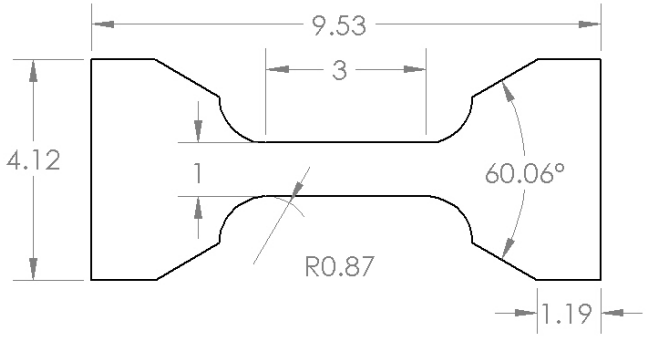

(f) tensile test sample dimensions (all dimension in mm)

Figure 1. Experimental set-up (cont.)

A four-factor, two-level, half-fractional DOE matrix was created as shown in Table 1, where A, B, C, and D denotes layer height, powder feed rate, energy density, and preheat condition, respectively.

Table 1. A 2_{IV}^{4-1} DOE matrix with the defining relation I=ABCD

Run No.	Basic Design			D=ABC	Treatment Combination
	A	B	C		
	mm	g/min	W/(mm/min)		
1	4	1.45	1.6	no preheat	(1)
2	6	1.45	1.6	preheat	ad
3	6	1.96	1.6	no preheat	ab
4	4	1.96	1.6	preheat	bd
5	6	1.45	1.7	no preheat	ac
6	4	1.45	1.7	preheat	cd
7	4	1.96	1.7	no preheat	bc
8	6	1.96	1.7	preheat	abcd

Final structures were then prepared with standard Ti-6Al-4V metallographic procedures [7] and etched with Kroll's reagent (92 ml distilled H2O, 6 ml HNO3, and 2 ml HF) for microstructure analyses. Vickers hardness distribution was evaluated along the build height direction with 0.05 kgf load, 30 s dwell time. Vickers hardness sampling points were distributed along three zigzag routes at 0.75 mm intervals and the Vickers hardness at certain positions was taken from the average VHN per each row with the same height. Tensile tests with sample size as shown in Figure 1f were conducted at test speed 0.015 mm/mm/min to evaluate the YS at 0.2% offset and the YS values were taken as the DOE response for the ANOVA test.

3. RESULTS AND DISCUSSION

The eight samples fabricated according to the DOE matrix are shown in Figure 2a. The microstructure from the deposit/substrate interface to the 12 mm height within the eight deposits was characterized. The characterization results showed grain boundary alpha, martensitic-alpha, and primary-alpha (colony and basketweave) morphologies, and basketweave was the typical type as depicted in Figure 2b to Figure 2e. Comparing the microstructure close to deposit/substrate interface and each machining boundary shows the deposit/substrate interface tends to have a finer α-lath than at the machining boundaries; for example, in Run 6, the average is 1.1 μm α-lath width at deposit/substrate interface and average 1.5 μm α-lath at each machining boundary. When samples were fabricated with the same layer height, but a high-level input energy density, a coarser α-lath tended to form near the machining boundary. This is demonstrated in Figure 2e by comparing the

microstructure near the first machining boundary from Run 3 and Run 5, where Run 3 has an average 1.4 μm α-lath width and Run 5 has an average 1.7 μm α-lath width.

For a higher input energy density, the results are consistent with that of a smaller the temperature gradient around the molten pool, resulting in a lower cooling rate across the beta-transus and into the alpha-beta phase field, leading to a coarser microstructure [8].

The observed microstructure near the machining boundary in the 6 mm layer height runs bear the same conclusions as drawn from the 4 mm layer height runs. The microstructure in all eight samples followed the same trend in that the average α-lath size was slightly larger as the distance from the substrate increased. Away from the boundaries, it was observed that a larger input energy density also tended to form a coarser microstructure within the deposits. Though the microstructure size varied as the evaluated height changed, there was no significant size difference normal to the build height direction.

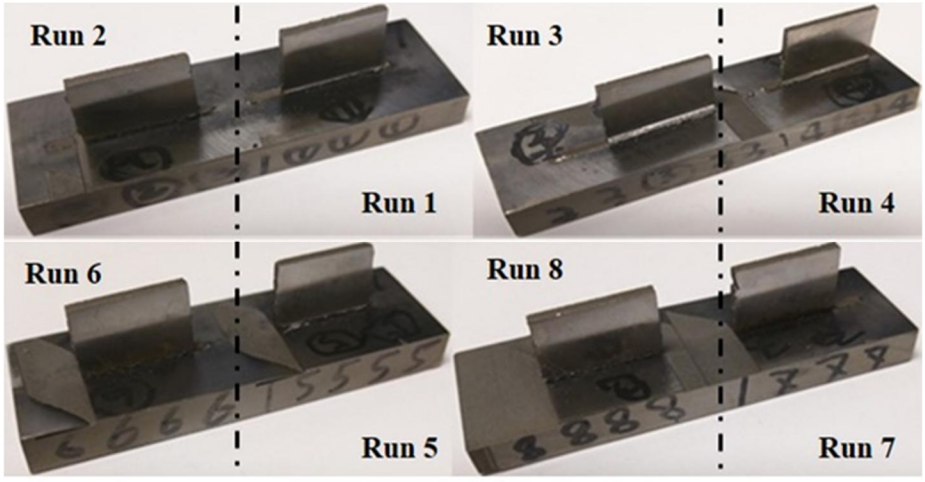

(a) thin-wall samples machined to the final dimension 20 mm x 2 mm x 12 mm

Figure 2. Material property characterization results

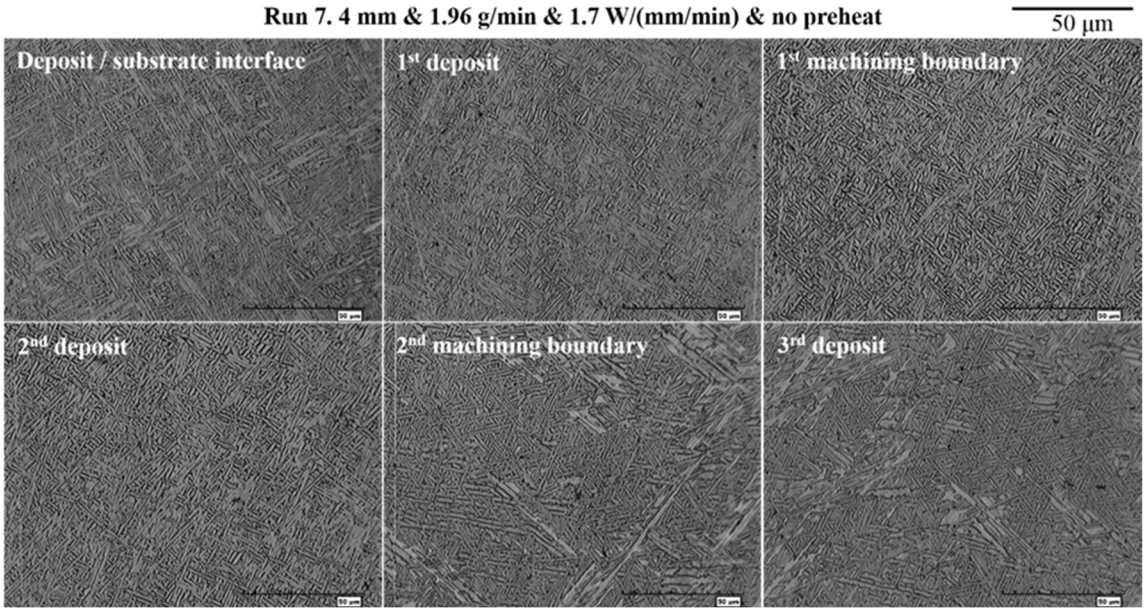

(b) typical microstructure at each deposit and machining boundary in Run 7

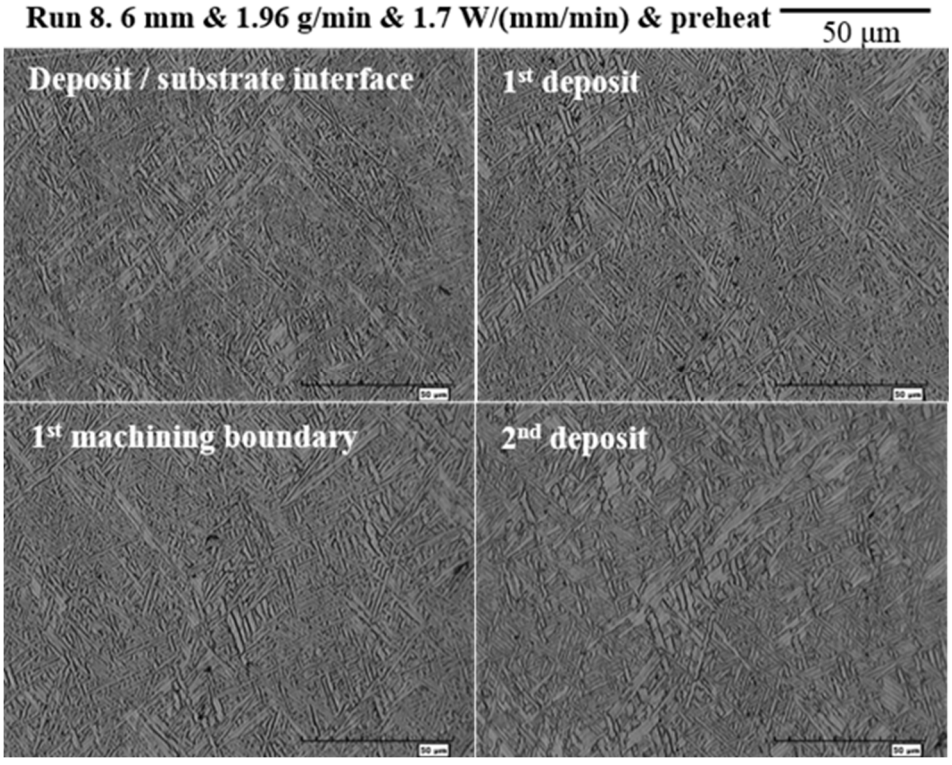

(c) typical microstructure at each deposit and machining boundary in Run 8

Figure 2. Material property characterization results (cont.)

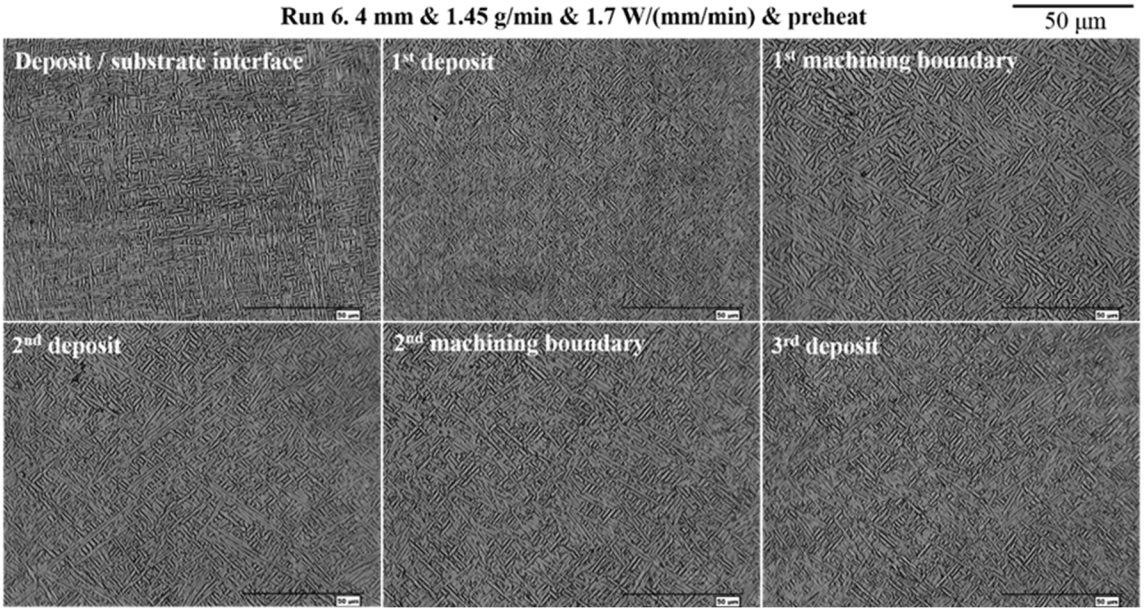

(d) typical microstructure at each deposit and machining boundary in Run 6

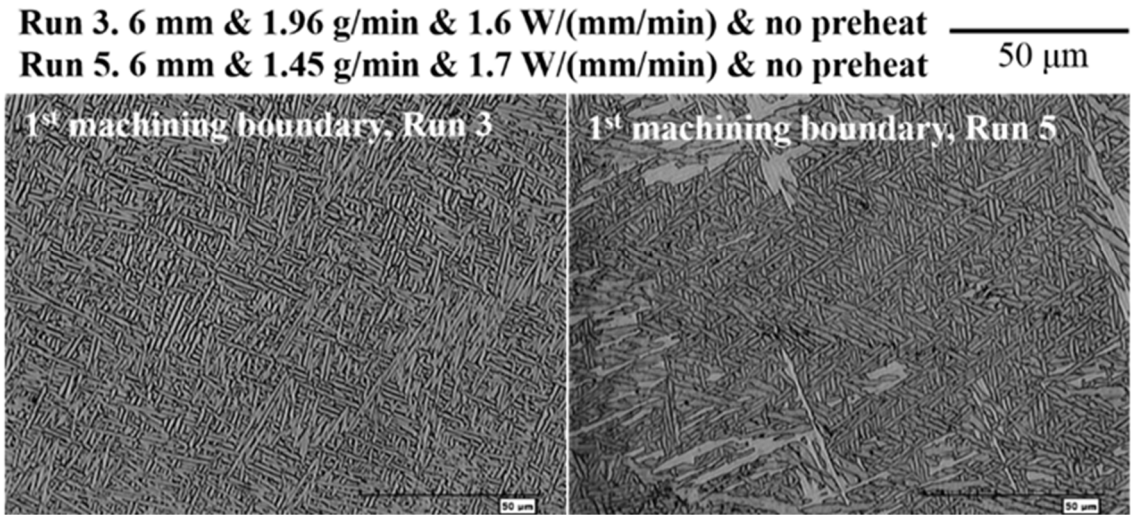

(e) microstructure comparison in Run 3 and Run 5 near the first machining boundary

Figure 2. Material property characterization results (cont.)

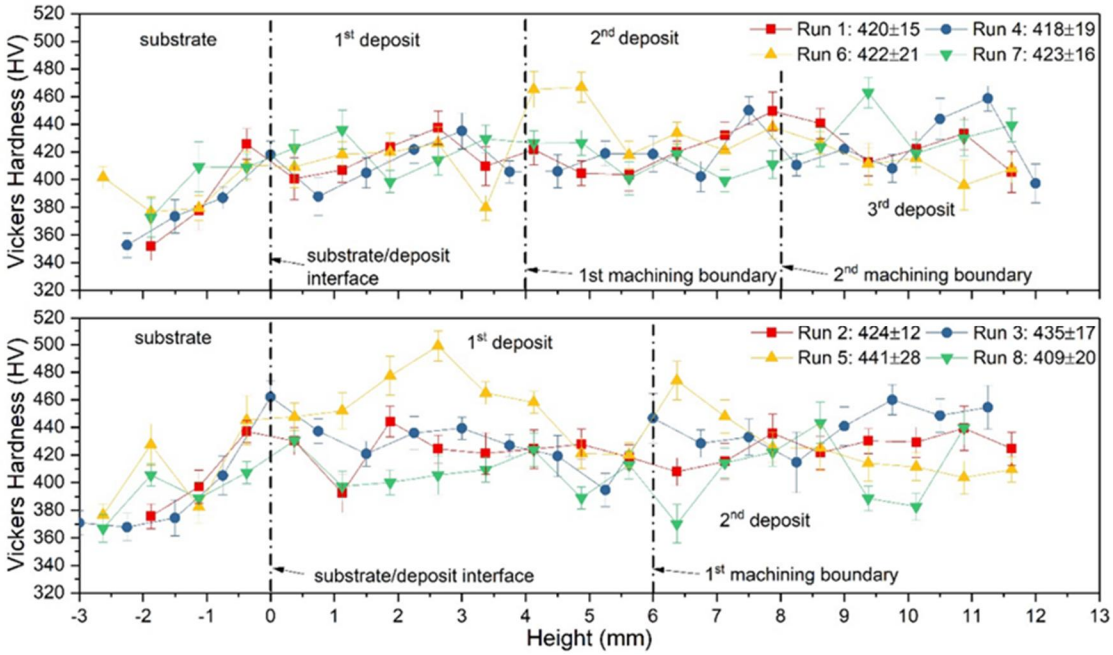

(f) Vickers hardness distribution along build height direction

Figure 2. Material property characterization results (cont.)

Because of the slow heat conduction of the thin-wall structure [8], the heat accumulated in the structure is unable to be rapidly transferred to the substrate and clamping fixture. The retained heat results in an annealing effect on the final part and leads to overall coarsening and homogenization of the α-lath sizes. The microstructure size difference was mostly observed in samples fabricated with different layer heights and input energy densities. Figure 2b shows the microstructure at different heights in Run 7, which had the same layer height and input energy density condition as Run 6, as shown in Figure 2d, and the minor microstructure size difference was seen in the comparison between them. The average Vickers hardness values shown in Figure 2f of the eight samples were labeled in the top right of the figure, and the data reveal that the Vickers hardness distribution followed a similar trend in the build height direction, which roughly reflects that the microstructure has a similar size distribution along build height direction. The chemistry

analysis will be needed to determine the sample oxygen content as the Vickers hardness and tensile strength increase as the oxygen concentration increase [9].

ANOVA test was conducted in SAS™ based on the YS data acquired from the tensile tests results shown in Table 2. The test was conducted according to the standard analyzing procedures of a four-factor, two-level, half-fractional design. The ANOVA test result shows that layer height, energy density, and the interaction of layer height and preheating condition significantly impacted the YS. The predicted YS model is described with significant factors and written as in Eq. 1:

$$YS = 965.9 + 23.3x_1 + 10.71x_3 - 52.96x_1 \times x_4 \quad (1)$$

where 965.9 is the average response and x_1, x_3, x_4 takes on values between -1 and 1, which denotes three selected factors: layer height, energy density, and preheat condition, respectively.

The response surface was generated by the YS regression model and is shown in Figure 3. Figure 3a shows the response surface contour plot when layer height was 6 mm ($x_1 = 1$), which indicates no preheat and high energy density tends to increase final part's YS. Figure 3b shows the response surface contour plot when preheat was applied ($x_4 = 1$), which indicates high energy density and low layer height tends to benefit the increase of YS values. The contour plot provides a detailed insight into the YS values with different processing parameter combinations.

To better understand the thermal history and resulting microstructure evolution, a validated FEA model for the in-house deposition system was implemented to explore the transient temperature history during the HM process [6]. Figure 4a and 4b show the built process of Run 6 and Run 8 and the evaluated point's location, which is along the deposit

center line, but with different heights. In both runs, points at the substrate's top surface and the middle height of each deposit was studied and their temperature history is plotted in Figure 4c. The machining between each deposition was modified by adding a 300 s cooling time after each deposition; it was experimentally validated that the deposits cool down to the ambient temperature after this time. The substrate top surface points reached a similar maximum temperature during the whole deposition process. In Run 8, the temperature increased more slowly in the second deposition period due to the layer height difference. The middle point of the first deposit in Run 6 had a similar maximum temperature during the second and third deposition period. The first deposit middle point in Run 8 had a slightly higher maximum temperature than in Run 6. Both points on the substrate top surface and in the middle of the first deposit had a minor response to the sudden change of temperature as the heat source passed it in the third deposition period for Run 6. The same conclusion can be drawn for the substrate top surface and the first deposit middle height points for Run 8. From the temperature history curves of points from Run 6 and 8, the maximum temperature increased as the deposit height increased and is retained in the build for an extended period of time due to the slow heat conduction of the thin-wall structure to the substrate and surrounding environment. The martensitic-alpha formed from 848 K when the cooling rate (CR) was greater than 410 K/s [8]. The colony formed at a lesser CR compared to the basketweave [8]. The basketweave formed when crossing the beta-transus temperature (~1173 K) when the CR was less than 20 K/s [10]. The evaluated points in the two runs all meet this criterion and are consistent with the resulting microstructure. Since maximum temperature exceeded the aluminum vaporization temperature, further chemistry analysis is required as aluminum is important to the α-lath formation and

distribution within the LMD part directly relates to the final product's mechanical properties [11]. The chemistry analysis results will also benefit processing window adjustment.

Table 2. Average YS at 0.2% offset of the eight samples

Run No.	YS (avg.) at 0.2% offset (MPa)
1	834
2	961
3	1022
4	1004
5	1049
6	1001
7	932
8	925

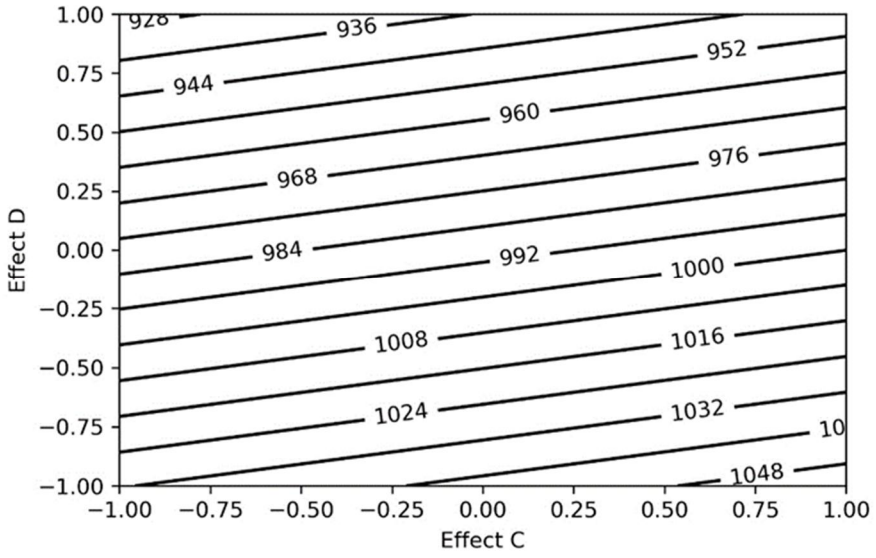

(a) contour plot of YS regression model with 6 mm layer height ($x_1 = 1$)

Figure 3. ANOVA test results

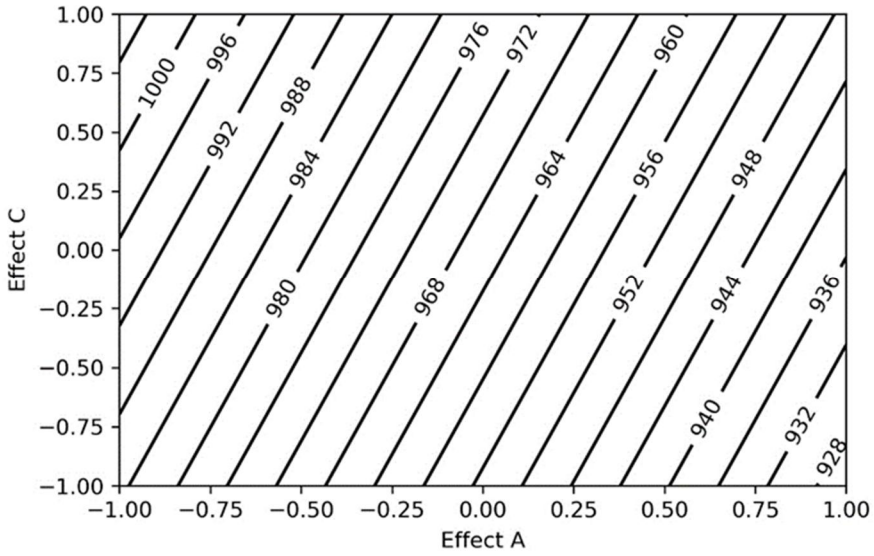

(b) contour plot of YS regression model with preheating condition ($x_4 = 1$)

Figure 3. ANOVA test results (cont.)

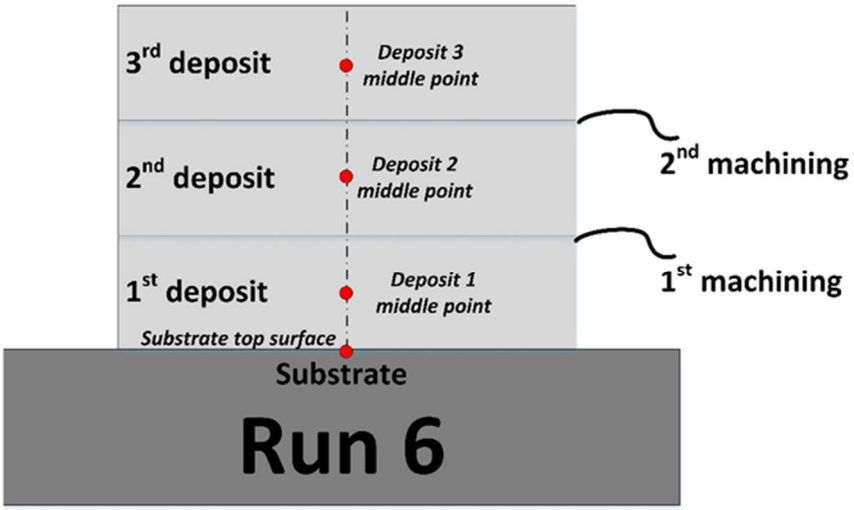

(a) built process for Run 6 and locations of the selected point for temperature evaluation

Figure 4. FEA simulation of Run 6 and Run 8

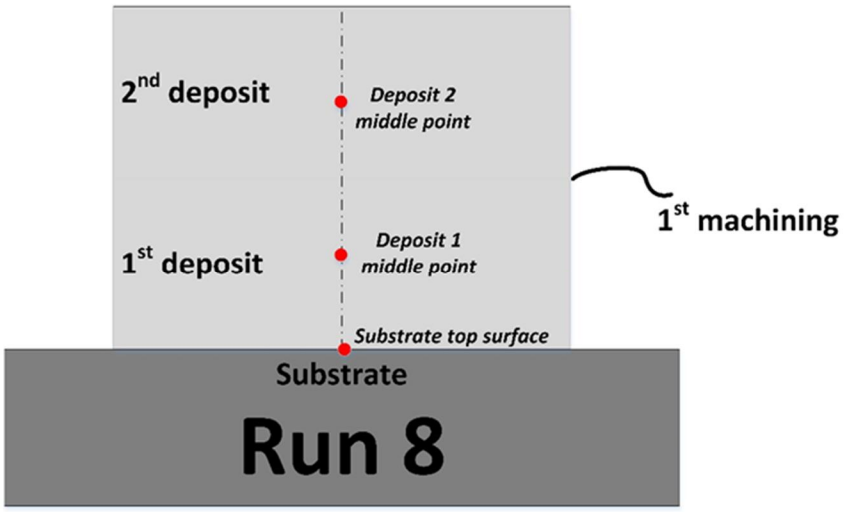

(b) built process for Run 8 and locations of the selected point for temperature evaluation

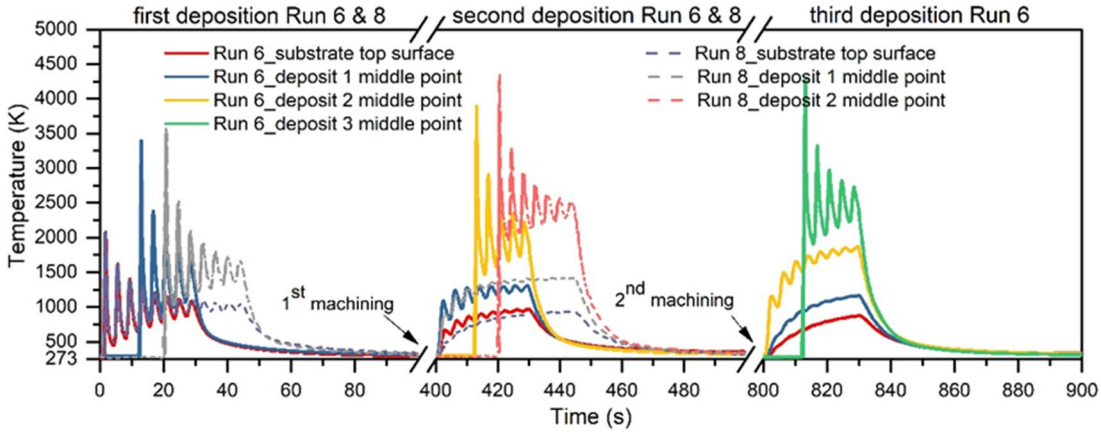

(c) temperature history at selected locations in Run 6 and Run 8

Figure 4. FEA simulation of Run 6 and Run 8 (cont.)

4. CONCLUSIONS

To conclude, the current work extends the understanding of the impact of parameters relevant to hybrid manufacturing on microstructure, Vickers hardness, and tensile test of Ti-6Al-4V. The following are the salient conclusions in the paper.

• Microstructure characterization reveals grain boundary alpha, martensitic-alpha, colony, and basketweave morphologies along the deposit build height direction.

• The average α-lath width at substrate/deposit interface is smaller than at machining boundaries; with the same layer height, coarser α-lath tends to form at machining boundaries at higher input energy density condition.

• Vickers hardness distribution within eight samples follows a similar trend along the build height direction.

• ANOVA test result shows layer height and input energy density have significant impacts on the yield strength, while powder feed rate and preheat condition do not for the parts fabricated in this work.

• A finite element analysis method was used to predict the transient temperature history of the deposit and shows the fulfillment of the criteria necessary for basketweave microstructure formation.

ACKNOWLEDGMENTS

This project was supported by The Boeing Company through the Center for Aerospace Manufacturing Technologies (CAMT), National Science Foundation Grants #CMMI-1547042 and CMMI-1625736, and the Intelligent Systems Center (ISC) at Missouri S&T. Their financial support is greatly appreciated.

REFERENCES

[1] Choi, Doo-Sun, S. H. Lee, B. S. Shin, K. H. Whang, Y. A. Song, S. H. Park, and H. S. Jee. "Development of a direct metal freeform fabrication technique using CO2 laser welding and milling technology," Journal of Materials Processing Technology 113, no. 1-3 (2001): 273-279.

[2] Hur, Junghoon, Kunwoo Lee, and Jongwon Kim. "Hybrid rapid prototyping system using machining and deposition," Computer-Aided Design 34, no. 10 (2002): 741-754.

[3] Akula, Sreenathbabu, and K. P. Karunakaran. "Hybrid adaptive layer manufacturing: An Intelligent art of direct metal rapid tooling process," Robotics and Computer-Integrated Manufacturing 22, no. 2 (2006): 113-123.

[4] Vasinonta, Aditad, J. L. Beuth, and Michelle Griffith. "Process maps for laser deposition of thin-walled structures," In Solid Freeform Fabrication Proceedings, pp. 383-391. The University of Texas at Austin, August, 1999.

[5] Salonitis, Konstantinos, Laurent D'Alvise, Babis Schoinochoritis, and Dimitrios Chantzis. "Additive manufacturing and post-processing simulation: laser cladding followed by high speed machining," The International Journal of Advanced Manufacturing Technology 85, no. 9-12 (2016): 2401-2411.

[6] Yan, Lei, Yunlu Zhang, and Frank Liou. "A conceptual design of residual stress reduction with multiple shape laser beams in direct laser deposition," Finite Elements in Analysis and Design 144 (2018): 30-37.

[7] Yan, Lei, Xueyang Chen, Wei Li, Joseph Newkirk, and Frank Liou. "Direct laser deposition of Ti-6Al-4V from elemental powder blends," Rapid Prototyping Journal 22, no. 5 (2016): 810-816.

[8] Kelly, S. M., and S. L. Kampe. "Microstructural evolution in laser-deposited multilayer Ti-6Al-4V builds: Part I. Microstructural characterization," Metallurgical and Materials Transactions A 35, no. 6 (2004): 1861-1867.

[9] Oh, J-M., B-G. Lee, S-W. Cho, S-W. Lee, G-S. Choi, and J-W. Lim. "Oxygen effects on the mechanical properties and lattice strain of Ti and Ti-6Al-4V," Metals and Materials International 17, no. 5 (2011): 733-736.

[10] Malinov, S., P. Markovsky, W. Sha, and Z. Guo. "Resistivity study and computer modelling of the isothermal transformation kinetics of Ti–6Al–4V and Ti–6Al–2Sn–4Zr–2Mo–0.08 Si alloys," Journal of Alloys and Compounds 314, no. 1-2 (2001): 181-192.

[11] Hayes, Brian J., Brian W. Martin, Brian Welk, Samuel J. Kuhr, Thomas K. Ales, David A. Brice, Iman Ghamarian et al. "Predicting tensile properties of Ti-6Al-4V produced via directed energy deposition," Acta Materialia 133 (2017): 120-133.

II. INVESTIGATION OF MACHINING COOLANT RESIDUE CLEANING METHODS FOR TI6AL4V PART FABRICATION THROUGH HYBRID MANUFACTURING PROCESS

Lei Yan[1], Yunlu Zhang[1], Joseph W. Newkirk[2], Frank Liou[1],
Eric E. Thomas[3], Andrew H. Baker[3]

[1]Department of Mechanical and Aerospace Engineering,
Missouri University of Science and Technology, Rolla, MO 65409
[2]Department of Materials Science and Engineering,
Missouri University of Science and Technology, Rolla, MO 65409
[3]The Boeing Company, St. Louis, MO 63043

ABSTRACT

A major concern in the hybrid manufacturing of Ti-6Al-4V parts is whether coolant residue from wet machining will cause contamination subsequent laser metal deposition operations. Laser rastering and compressed air were used in a cleaning effectiveness study with oil- and water-based coolant residue. The cleaning effect was evaluated by Vickers hardness and tensile tests on parts which were built on cleaned surfaces by the aforementioned methods. The conclusions, drawn from comparison with deposit built on dry machining surface, indicates laser heating for thin oil-based coolant residue and laser heating then cleaning with compressed air for water-based coolant residue yield good cleaning effectiveness.

Keywords: Ti-6Al-4V; Coolant Residue; Hybrid Manufacturing; Laser Heating; Compressed Air

1. INTRODUCTION

Hybrid manufacturing (HM) combines the freedom of additive manufacturing with the precision of computer numerical control (CNC) machining to enable done-in-one ability, which allows in-process quality inspection, speeds up production of complex metal parts, and overcomes the difficulty in machining inner features. In recent years, several HM systems have been developed, SLS/SLM with milling [1], arc welding with milling [2-5], and machining center with LENS® function. Recent research is only focused on machining technology improvement for the final parts fabricated through additive manufacturing [6-7]. To the best of our knowledge, no research has been focused on coolant residue cleaning within the machining and laser deposition sequence. It is critical to find an appropriate coolant residue cleaning method that maintains final part's mechanical performance and improves efficiency in production. Although feasibility research with dry machining on additively manufactured Ti-6Al-4V parts has been performed [8], the low feed rate to achieve the same surface integrity with coolant applied is not suitable for industrial production. Oil- and water-based coolant are the most common coolant types in Ti-6Al-4V machining [6-7]. Acetone was considered for an oil-based coolant residue removal method for its good degreasing ability and quick evaporation, but it was eliminated from consideration since the cleaning process is performed in the HM machine and the acetone will dry out or damage the system's seals. To avoid involved additional efforts, laser rastering and compressed air embedded in the HM machine are

considered for coolant residue cleaning. In this work, both oil- and water-based coolant have been tested in four scenarios, where different combinations of laser heating and compressed air for coolant residue cleaning were implemented. Deposits built within the four scenarios are compared with samples deposited on dry machined surfaces by evaluating Vickers hardness and tensile test results. The results will help to provide guidelines for HM process production improvement.

2. EXPERIMENTAL PROCEDURES

Both oil- and water-based coolant have been tested with different cleaning methods along with a no-coolant condition as a benchmark for comparison. All the scenarios are listed in Table 1. Gas atomized Ti-6Al-4V powders (Advanced Specialty Metals, NH, USA) with size -60+120 mesh is used for all the deposition. Grade 5 Ti-6Al-4V plates (ATI, PA, USA) with dimension 75 mm x 25 mm x 7 mm are used as substrates. Thermogravimetric analysis (TGA) was employed first to verify the feasibility of whether heating can burn off the coolant residue and at what temperature coolant residue can be removed. TGA samples as shown in Figure 1a were EDM cut into thin disks with a diameter of 5 mm and a thickness of 0.2-0.3 mm from the aforementioned Ti-6Al-4V plate, brushed coolant on one side, then tested at argon environment with a heating rate of 100 ^{0}C /min (the maximum heating rate of the TGA equipment). Based on the TGA results, using laser heating with appropriate laser power to burn off coolant residue is feasible, and therefore the subsequent test-matrix evaluating laser heating as a cleaning method was executed.

Laser scanning along the deposition path was applied with a laser power of 200 W, a beam diameter of 1mm, and a scanning speed of 216 mm/min. Coolant was brushed on

the machined surface to simulate the after-machining condition of a part fabricated using the HM process. Compressed air (90-100 psi) cleaning before laser heating is not considered for the oil-based coolant trial as the coolant residue on the machined surface was blown with compressed air for one minute and visually made almost no changes due to the high viscosity of the coolant.

Table 1. Coolant residue cleaning scenarios

Scenarios No.	Coolant Type	Experiment Procedure
1	No coolant	Step 1: Deposit
2	Oil-based (Hocut 795B)	Step 1: Brush coolant on machined surface Step 2: Laser Heating Step 3: Deposit
3		Step 1: Brush coolant on machined surface Step 2: Laser Heating Step 3: Compressed air cleaning laser scanned surface Step 4: Deposit
4	Water-based	Step 1: Brush coolant on machined surface Step 2: Compressed air drying machined surface Step 3: Laser Heating Step 4: Deposit
5		Step 1: Brush coolant on machined surface Step 2: Laser Heating Step 3: Deposit

Except for the five scenarios in Table 1, two additional scenarios with no cleaning procedures conducted on the machined surfaces were also tested, which means deposits were directly built on the machined surfaces after coolant was brushed.

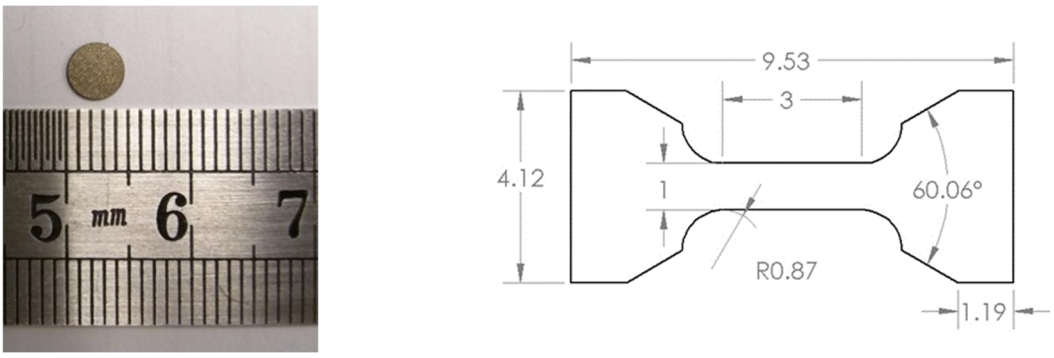

(a) TGA sample (b) mini tensile test sample dimension (all dimensions in mm)

Figure 1. TGA and mini tensile test sample dimension

Vickers hardness and tensile testing were conducted to evaluate the cleaning effectiveness of the four cleaning methods. Cross section of the deposits and substrates were EDM cut, mounted, and polished according to the standard Ti-6Al-4V metallographic procedure [9], then tested with 0.05 kgf load and 30 s dwell time along the deposition height direction. Mini tensile test samples were EDM cut according to the dimensions shown in Figure 1b and polished with 800 grit sandpaper to remove microcracks within the gauge length before testing.

3. RESULTS AND DISCUSSIONS

The TGA results of water- and oil-based coolant are shown in Figure 2. Figure 2a shows the water-based coolant TGA thermal curve and the 1st derivative curve as an inset, where the weight loss rate reaches zero at 450 ^{0}C. Sample weight difference before coolant

was introduced and after coolant was burnt off is less than 0.5%. Figure 2b shows the oil-based coolant TGA results, where the weight loss rate reaches zero at 500 ^{0}C. The sample weight difference before coolant was introduced and after coolant was burnt off is less than 0.8%. The minor weight difference indicates heating has positive effects on coolant residue cleaning. In both cases, two inflection points in the 1st derivative curve are observed, which indicate the two greatest rates of weight change. In future testing, TGA-FT-IR (Infrared Spectrometer) will be employed to identify the components at each inflection points.

The temperature history along the scanning path during laser heating process was investigated with a three-dimensional finite element model [10], which predicts the peak temperature is around 1500 K and is higher than the maximum temperatures tested with the TGA method. Vickers hardness was measured along the height direction, defined from the substrate to the top of the deposit. As shown in Figure 2c, two scenarios, scenario 3 and 5, have higher hardness values than scenario 1 in the first 1.5 mm of the deposits, which may come from an interaction between the coolant and the initial deposition layer. This interaction would be due to laser heating at a temperature insufficient to completely remove the coolant residue outside of the laser passes. The Vickers hardness distribution of the other two scenarios has a good alignment with the no coolant scenario and demonstrates that the methods used for coolant residue removal have little effect on hardness.

Figure 2d presents the tensile test results, which clearly depicts scenario 5 having lower values of yield strength (YS) and ultimate tensile strength (UTS) values compared to the baseline scenario 1. Compared to scenario 1, the YS differences are within 1% for the other scenarios.

Microstructure near deposit and substrate boundary was compared as shown in Figure 3a to Figure 3e, where basketweave is the typical microstructure type and all evaluated scenarios have very similar grain size.

The typical defects observed in the two additional scenarios with no cleaning methods conducted are cracks and contaminations as shown in Figure 3f. Due to the massive cracks observed near the interface between the substrate and as-built wall then no tensile and hardness tests were conducted. Further research will focus on chemical analyses of the failed deposits to figure out reasons for defects generation.

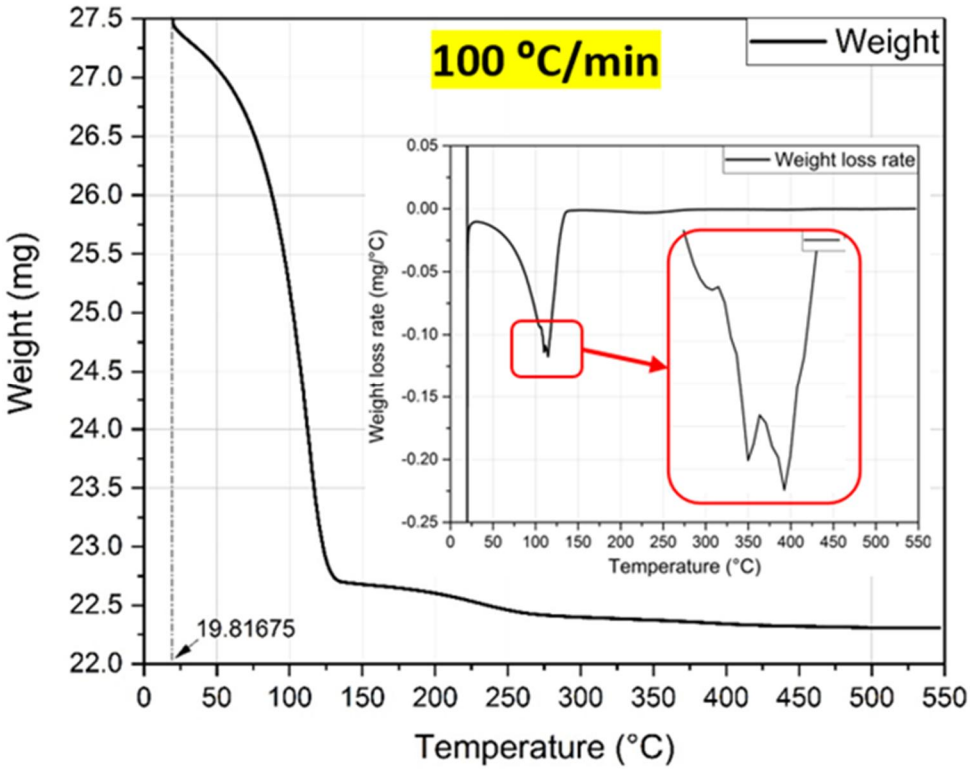

(a) water-based coolant TGA analysis results

Figure 2. Analyses results

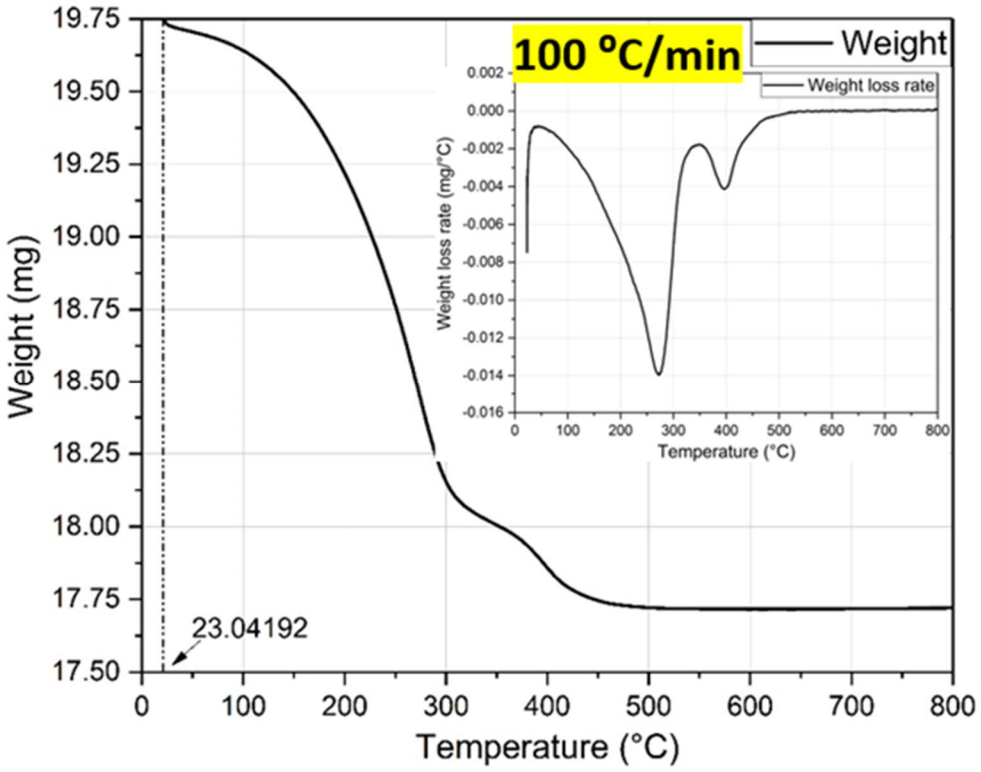

(b) oil-based coolant TGA analysis results

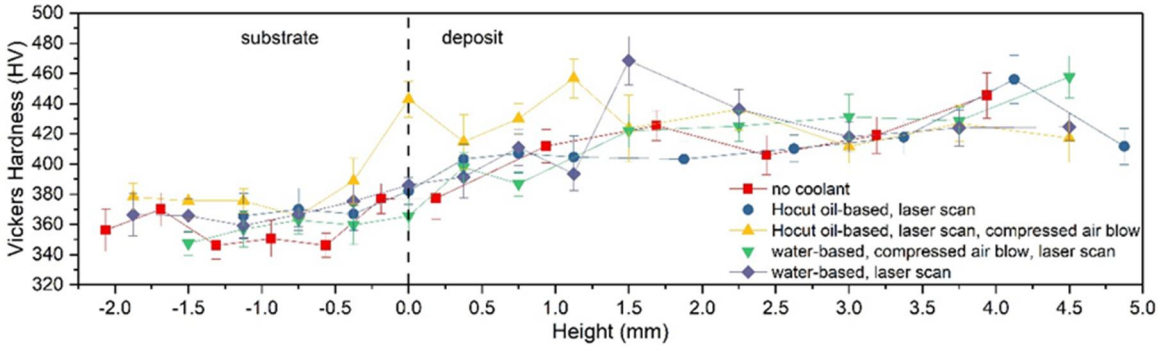

(c) Vickers hardness results

Figure 2. Analyses results (cont.)

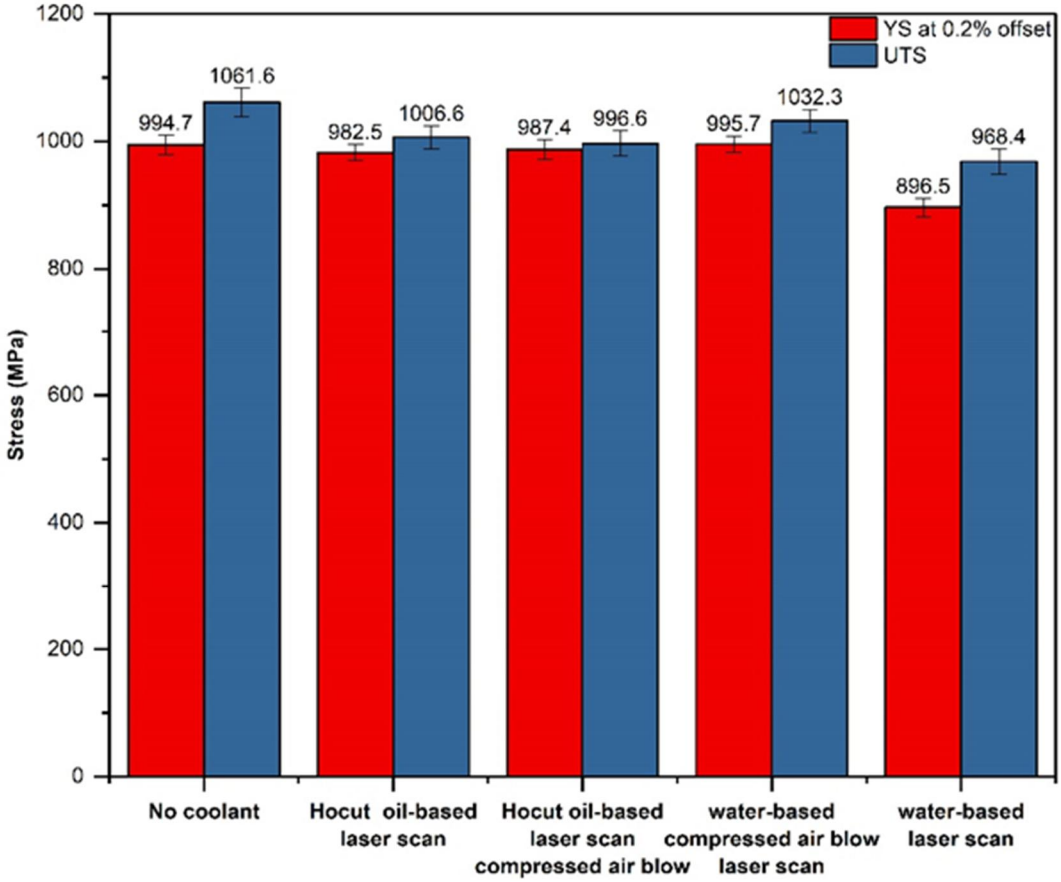

(d) Tensile test results. Error bars in the Vickers hardness and tensile test data show one standard deviation

Figure 2. Analyses results (cont.)

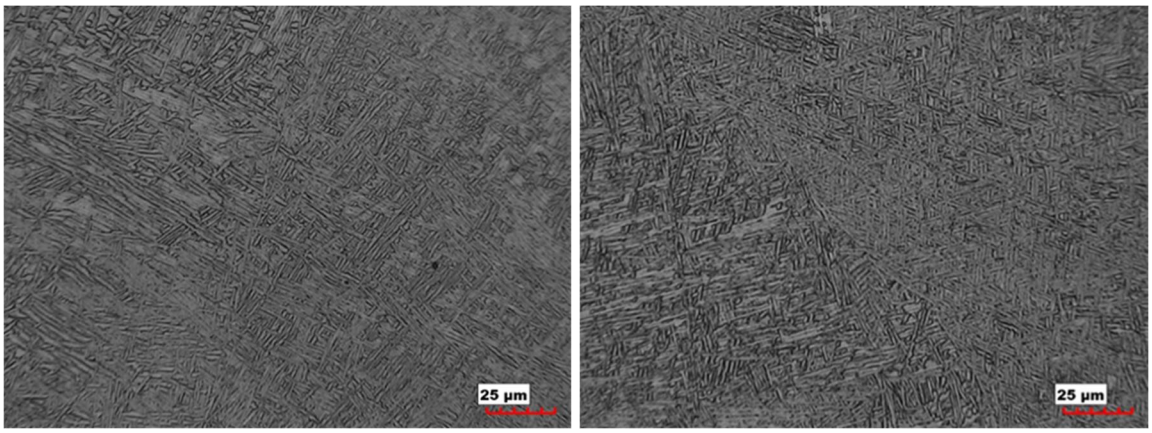

(a) scenario 1 (b) scenario 2

Figure 3. Microstructure near deposit and substrate boundary

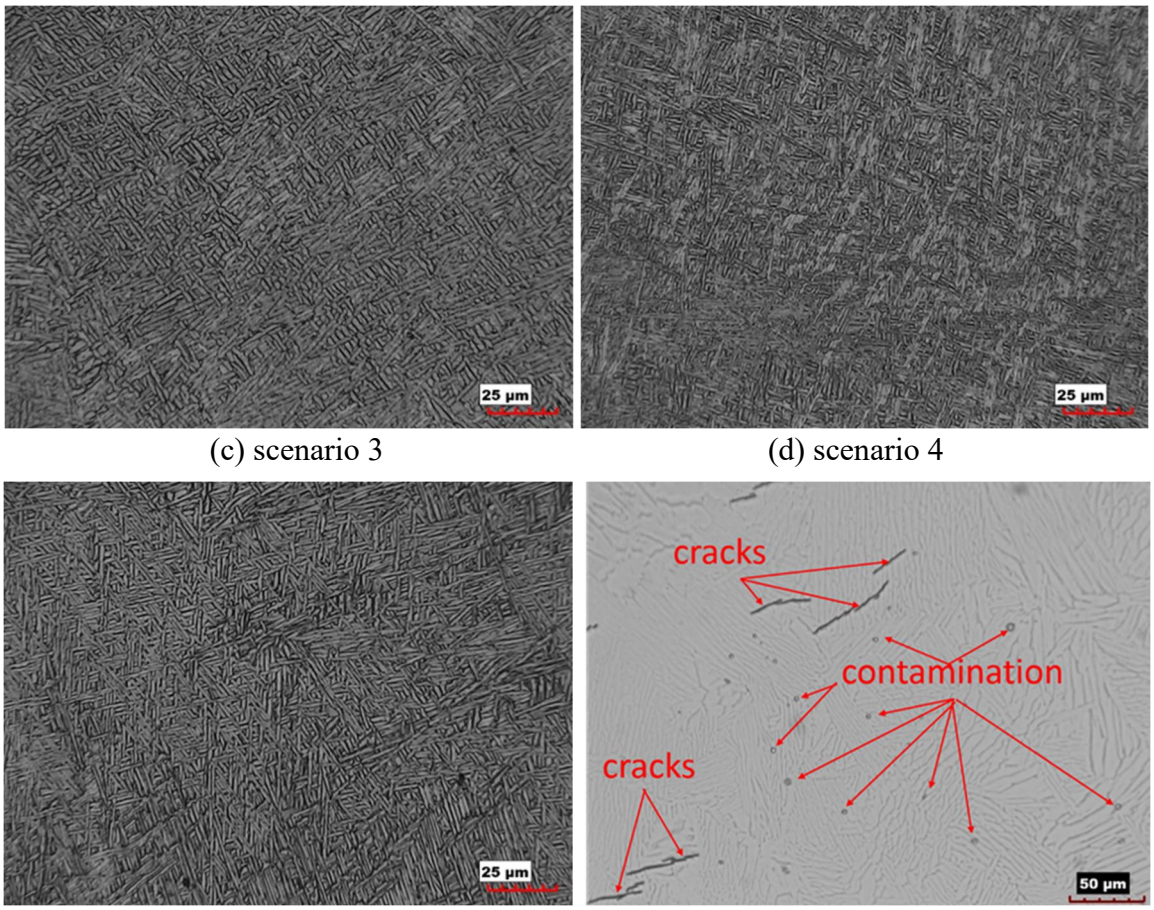

(c) scenario 3 (d) scenario 4

(e) scenario 5 (f) scenario 6

Figure 3. Microstructure near deposit and substrate boundary (cont.)

4. CONCLUSIONS

The current research was implemented to investigate the elemental powder effect on composition control for as-deposited parts via the LMD process. By using the suitable condition, the target alloy using elemental powder mixture can be obtained, which ensures the analyses of the elemental powder distributions. The fabricated Ti-6Al-4V alloy from Ti, Al, and V powder mixture was characterized using techniques such as optical microscopy, electron microscopy, hardness testing. It proves that the industry qualified Ti-6Al-4V alloy could be obtained by using elemental powder mixture with designed

proportions. Furthermore, this method can be used for fabrication of other alloys by using elemental powder mixture.

In this work, water- and oil-based coolant residue cleaning methods were investigated. The cleaning effectiveness was evaluated by Vickers hardness and mini tensile test results. The main outcomes of this work are summarized as follows:

1. Feasible methods for both oil-based and water-based coolant cleaning in HM process for Ti-6Al-4V parts have been obtained.
2. Laser heating and compressed air followed by laser heating can effectively clean oil- and water-based coolant residue without sacrificing tensile properties.

ACKNOWLEDGMENTS

This project was supported by The Boeing Company through the Center for Aerospace Manufacturing Technologies (CAMT), National Science Foundation Grants #CMMI-1547042 and CMMI-1625736, and the Intelligent Systems Center (ISC) at Missouri S&T. Their financial support is greatly appreciated.

REFERENCES

[1] Ye, Zhi-peng, Zhi-jing Zhang, Xin Jin, Mu-Zheng Xiao, and Jiang-zhou Su. "Study of hybrid additive manufacturing based on pulse laser wire depositing and milling," The International Journal of Advanced Manufacturing Technology 88, no. 5-8 (2017): 2237-2248.

[2] Xiong, Xinhong, Haiou Zhang, and Guilan Wang. "Metal direct prototyping by using hybrid plasma deposition and milling," journal of materials processing technology 209, no. 1 (2009): 124-130..

[3] Xiong, Xinhong, Zhang Haiou, and Wang Guilan. "A new method of direct metal prototyping: hybrid plasma deposition and milling," Rapid Prototyping Journal 14, no. 1 (2008): 53-56.

[4] Song, Yong-Ak, and Sehyung Park. "Experimental investigations into rapid prototyping of composites by novel hybrid deposition process," Journal of Materials Processing Technology 171, no. 1 (2006): 35-40.

[5] Karunakaran, K. P., S. Suryakumar, Vishal Pushpa, and Sreenathbabu Akula. "Retrofitment of a CNC machine for hybrid layered manufacturing," The International Journal of Advanced Manufacturing Technology 45, no. 7-8 (2009): 690-703.

[6] Pramanik, Alokesh, and Guy Littlefair. "Machining of titanium alloy (Ti-6Al-4V)—theory to application," Machining science and technology 19, no. 1 (2015): 1-49.

[7] Pramanik, Alokesh. "Problems and solutions in machining of titanium alloys," The International Journal of Advanced Manufacturing Technology 70, no. 5-8 (2014): 919-928.

[8] Bordin, A., S. Sartori, S. Bruschi, and A. Ghiotti. "Experimental investigation on the feasibility of dry and cryogenic machining as sustainable strategies when turning Ti6Al4V produced by Additive Manufacturing," Journal of cleaner production 142 (2017): 4142-4151.

[9] Yan, Lei, Xueyang Chen, Wei Li, Joseph Newkirk, and Frank Liou. "Direct laser deposition of Ti-6Al-4V from elemental powder blends," Rapid Prototyping Journal 22, no. 5 (2016): 810-816.

[10] Yan, Lei, Wei Li, Xueyang Chen, Yunlu Zhang, Joe Newkirk, Frank Liou, and David Dietrich. "Simulation of Cooling Rate Effects on Ti–48Al–2Cr–2Nb Crack Formation in Direct Laser Deposition." Jom 69, no. 3 (2017): 586-591.

III. FAST PREDICTION OF THERMAL HISTORY IN LARGE-SCALE PARTS FABRICATED VIA A LASER METAL DEPOSITION PROCESS

Lei Yan[1], Joseph W. Newkirk[2], Frank Liou[1],
Eric E. Thomas[3], Andrew H. Baker[3], James B. Castle[3]

[1]Department of Mechanical and Aerospace Engineering,
Missouri University of Science and Technology, Rolla, MO 65409
[2]Department of Materials Science and Engineering,
Missouri University of Science and Technology, Rolla, MO 65409
[3]The Boeing Company, St. Louis, MO 63043

ABSTRACT

Laser metal deposition (LMD) has become a popular choice for the fabrication of near-net shape complex parts. Plastic deformation and residual stresses are common phenomena that are generated from the intrinsic large thermal gradients and high cooling rates in the process. Finite element analysis (FEA) is often used to predict the transient thermal cycle and optimize processing parameters; however, the process of predicting the thermal history in the LMD process with the FEA method is usually time-consuming, especially for large-scale parts. Herein, multiple 3D FEA models with simple assumptions on the heat source and its loading methods are compared and validated with experimental thermocouple data.

Keywords: Laser Metal Deposition; Finite Element Analysis; Heat source; Thermocouple

1. INTRODUCTION

In the laser metal deposition (LMD) process, a description of the transient temperature fields is important for subsequent analyses such as microstructure evolution, residual stress, and distortion. Many efforts have been put on the temperature field analysis and are mainly based on the finite element analysis (FEA) method [1-5]. In literature, a commonly used method to mimic the material addition process is called the "dummy material method" [3] or the "element birth and death method" [5], which use active elements in the finite element model according to a predefined deposition strategy. The aforementioned methods usually include a computational intensive model as not only do the minimum required time increments in transient heat transfer analysis need to be met [6], but also a mesh convergence needs to be achieved, which requires a minimum element size relative to the laser beam diameter [5]. When applied, the conventional methods to predict transient temperature history in a large-scale part fabrication process increase the model size tremendously. In some cases, a precise description of the thermal history in the laser deposition process is not necessary and only a fast prediction of the peak temperature will be needed for the process plan. Herein, two methods called track-heat-source and layer-heat-source are proposed for fast prediction of transient thermal history in large-scale part fabrication via the LMD process.

2. EXPERIMENTAL SET-UP AND METHODS

A Ti-6Al-4V block was built on a DMG-Mori Lasertec 4300 3D hybrid machine with the following processing parameters: laser power 1680 W, laser beam spot size 4 mm, powder feed rate 29.7 g/min, and travel speed 1000 mm/min. The experimental set-up is

shown in Figure 1. Figure 1a shows the thermocouple locations on the substrate. The deposit was fabricated according to the path plan shown in Figure 1b, where nine single-direction laser scans were applied and a perimeter pass was performed on every layer. To provide a flat deposition on all corner walls, the perimeter pass was doubled every other layer based on trial-and-error. Figure 1c shows the thermocouples were fixed on the substrate with high temperature thermally conductive paste and temperature was recorded with a data acquisition instrument. Two holes shown in Figure 1c were used for mounting the substrate on a base plate. The final product is shown in Figure 1d. Due to the working condition differences among varies LMD systems, there is no comparison with other groups' work and only focused on the experimental data obtained from our LMD system. To quickly predict the transient thermal history of a large-scale part build on this machine, an FEA model suitable for this process was developed and the predicted temperature fields will be used for subsequent analyses such as oxidation, residual stress, and distortion in the future.

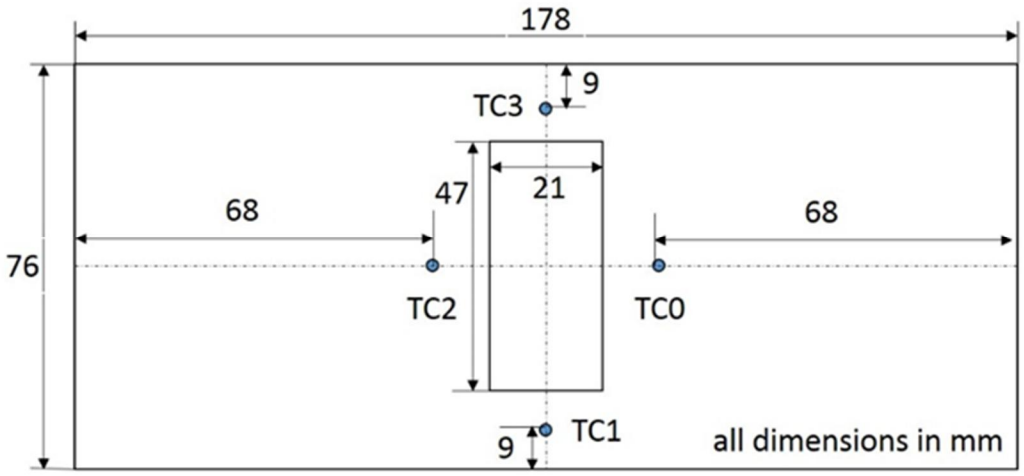

(a) thermocouple locations

Figure 1. Experimental set-up

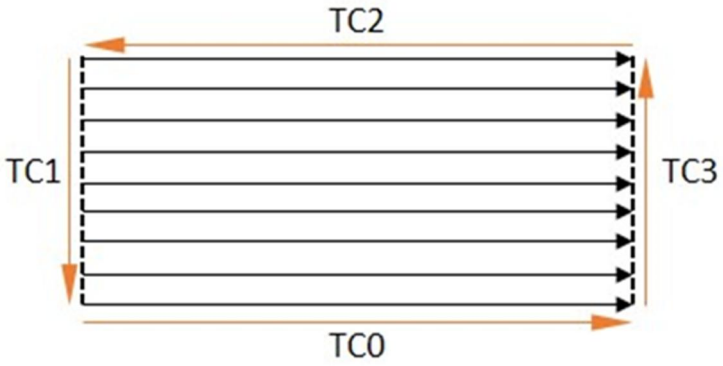

(b) laser scanning pattern

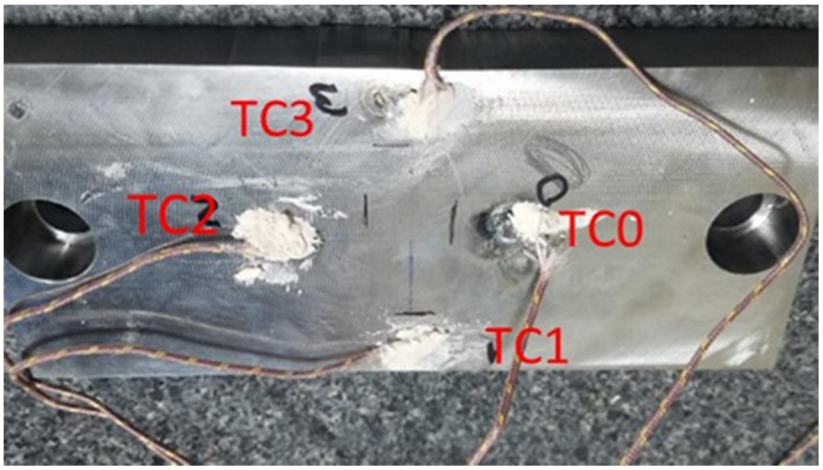

(c) thermocouples on the substrate before deposition

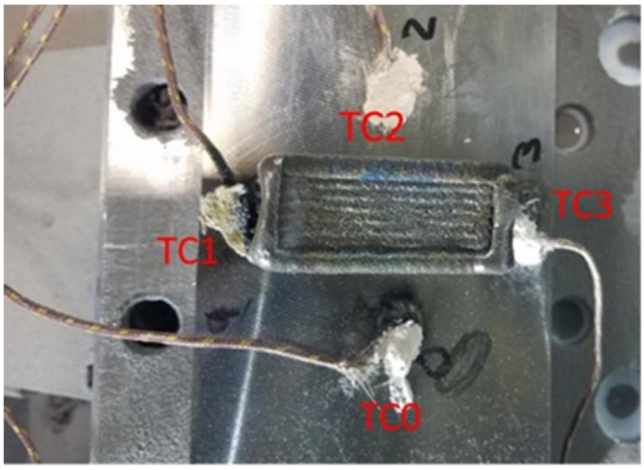

(d) final deposit

Figure 1. Experimental set-up (cont.)

3. MODELING PROCEDURES

In our previous work of simulating the LMD process, the heat source was modeled with a conventional method as thermal flux density (watt/m^2) or heat generation rate (watt/m^3) that moves place to place according to a scanning strategy [5,7], which requires a minimum element size (<1/6 laser beam diameter) to meet the requirement of mesh convergence assessment. This criteria results in a large number of elements and nodes in the meshed model and results in a long simulation time. To reduce the model size and computational time, and make it feasible for fast prediction of the temperature in the LMD process, especially for large-scale parts, some assumptions and simplifications were proposed and implemented in the model:

1. In the finite element model, the thermal load in both track- and layer-heat-source scenarios are applied sequentially in the form of thermal flux density and volume heat generation rates.
2. Thermal flux density is applied in the first seconds ((beam diameter)/(laser transverse speed)) with the maximum energy intensity value of the corresponding Gaussian beam.
3. Volume heat generation rate is applied in the rest of the time within each track or each layer with an average value calculated by absorbed energy divided by the deposited volume.

The finite element model was implemented by solving the following heat transfer equations. The governing equation of 3D heat transfer is given in Eq. (1):

$$\nabla \cdot k\nabla T + \dot{q} = \rho c_p \frac{\partial T}{\partial t} \tag{1}$$

where T is temperature, t is time, c_p is specific heat at constant pressure, ρ is density, k is thermal conductivity, and ∇ is the Hamilton operator which is equal to $(\partial/\partial x, \partial/\partial y, \partial/\partial z)$. There was no internal heat generation, so the $\dot{q}$ was set to zero. Density, thermal conductivity, and specific heat were all implemented as temperature-dependent parameters. Latent heat effects were modeled using Eq. (2) [8].

$$c_p^*(T) = c_p(T) + \frac{L}{T_m - T_0} \tag{2}$$

where $c_p^*(T)$ is the modified specific heat, $c_p(T)$ is the temperature-dependent specific heat, L is the latent heat of fusion, T_m is the melting temperature, and T_0 is the ambient temperature. The temperature-dependent property values of the Ti-6Al-4V substrate and deposit were taken from [9].

Fixtures play an important role as heat sinks in the laser deposition process [5]. In the current model, two bolts were simplified as two blocks at two ends of the substrate, and the base plate underneath the substrate was also modeled as a block, as shown in Figure 2a, where their material properties were assigned using the equivalent mass method as proposed in [5]; mass, thermal conductivity, and specific heat were kept the same, but density was modified according to the modeled fixture volume. As shown in Figure 2a, the model was meshed with a non-uniform distributed element size and only used fine mesh at volumes of interest to reduce the model size and computational time. The final model contains total 14922 elements and 17150 nodes.

The initial condition for the numerical simulation domain was set to a uniform temperature field equal to ambient temperature (300 K), which is defined as shown in (3).

$$T|_{t=0} = T_0, 0 \le x \le L_1, 0 \le y \le L_2, 0 \le z \le L_3 \tag{3}$$

The boundary conditions for all surfaces (both substrate and deposit) were set to have convection and radiation losses (4) [7]:

$$k(\nabla T \cdot \vec{n})|_{\Omega} = h(T - T_a)|_{\Omega} + \varepsilon\sigma(T^4 - T_e^4)|_{\Omega} - Q_r|_{\Omega laser} \quad (4)$$

where h was convective heat transfer coefficient, T_a was the ambient temperature, ε was emission coefficient, σ was the Stefan-Boltzmann constant ($5.67 \times 10^{-8}\, W/m^2K^4$), T_e was the wall temperature of the sealed chamber and set equal to T_a, and $Q_r$the is the heat input from the laser beam. As new elements changed from death to birth status, the outer surfaces related to boundary conditions were updated.

In this case, forced convection needs to be considered as reported in [10], where the decrease of as the distance from the top edge of the wall increases was assumed to be linear as provided in (5):

$$h = -1.4z + 80 \quad (5)$$

where z is the distance from the top edge of the wall to the point of interest. The convective heat transfer coefficient distribution at the last step is shown in Figure 2b, where the substrate and fixture were set to free convection when z was beyond the deposit height and the convective heat transfer coefficient was equal to 30 W/m^2/°C.

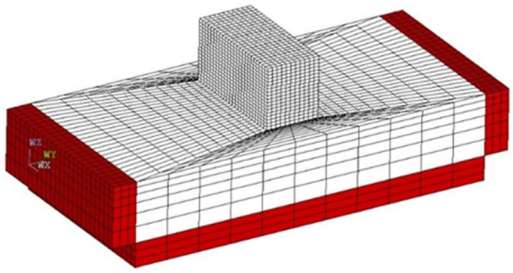

(a) meshed mode with the simplified fixture (red), the part (white)

Figure 2. FEA model set-up

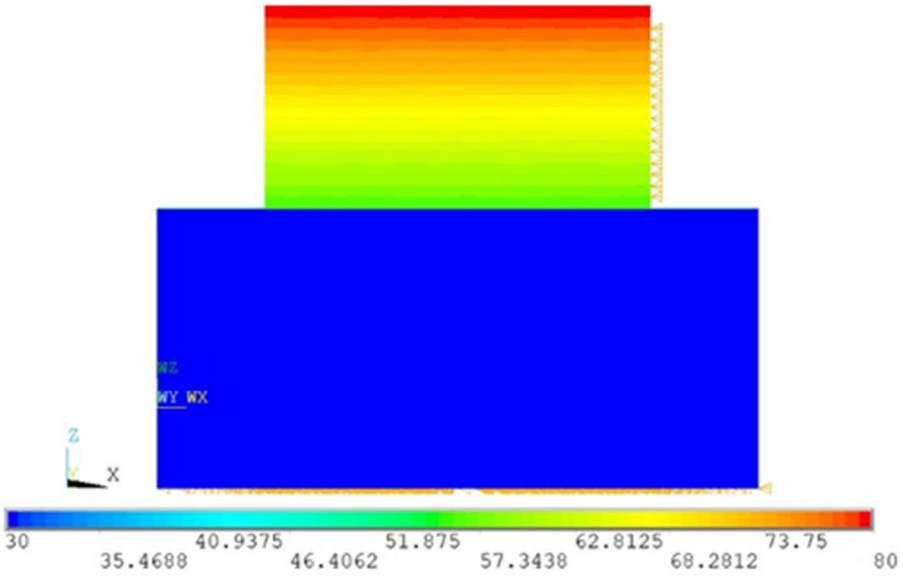

(b) convection coefficient distribution

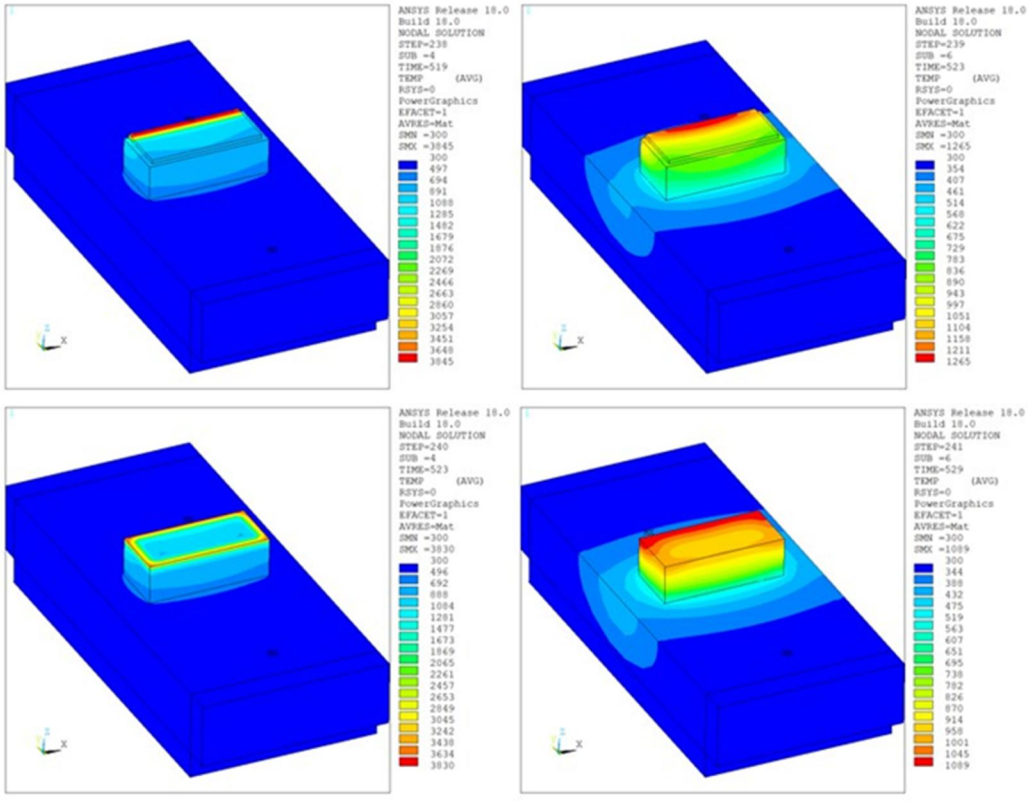

(c) temperature distribution at 11th layer with track heat source

Figure 2. FEA model set-up (cont.)

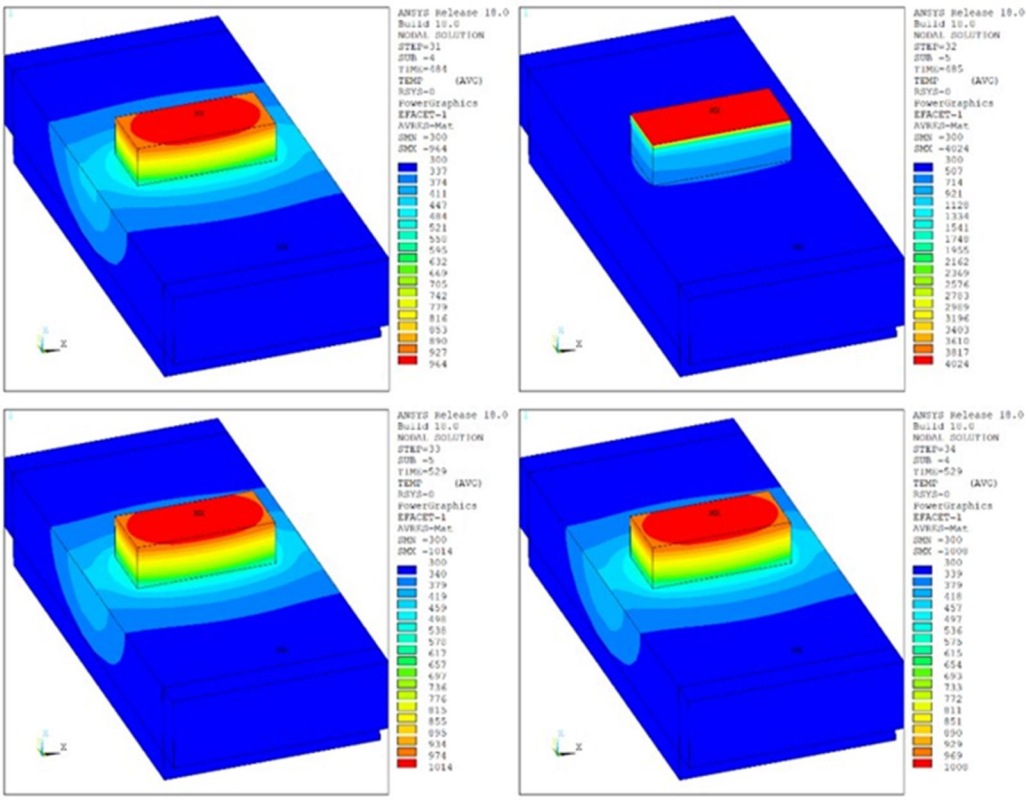

(d) temperature distribution at 11th layer with layer heat source

Figure 2. FEA model set-up (cont.)

The finite element model uses a fixed mesh size for all the substrates, deposits, and fixtures during simulation. To simulate the addition of material in the laser deposition process, a method called element birth and death in ANSYS was employed. The element death function was used to deactivate an element by setting its stiffness to zero, while the element birth function was used to activate an element by setting the right stiffness value. At the start of the simulation, the substrate elements were all activated. However, the deposit elements were activated sequentially to simulate material addition. The element birth and death method application in track-heat-source and layer-heat-source are demonstrated in Figure 2c and 2d, respectively. Figure 2c shows the tracked heat source

process where the heat flux was applied to the last track of the 11th layer, followed by the volume heat generation rate. The perimeter scan was simulated after the last track was added, following the same heat source application sequence as the last track. In Figure 3d, the layered heat source process is shown, with the only difference from the track-heat-source method being the material was added layer by layer instead of track by track.

4. RESULTS AND CONCLUSIONS

The predicted transient thermal history from the FEA model was validated with the thermocouple data and the comparison results are shown in Figure 3. TC1 was caught in the laser path during deposition and its measured data was peaked out. Only TC0, TC2, and TC3 measured data were used in the model validation process. The comparison between TC0, TC2, and TC3 is plotted in Figure 3a, which shows some variance from 0 to approximately 150 seconds and aligns well after that until the end of deposition. The mismatch around 150 seconds is attributed to the difference in loading method in simulation and reality. In simulation, the heat source was applied track by track, but in reality the heat source (laser beam) started from one end and moved to the other end of each track, which led to the locations where the thermocouples were attached to be heated up gradually and reached a peak temperature every time the laser beam passed over. After certain layers, the substrate was heated up and the temperature difference caused by the loading methods was reduced. Heat input and heat loss at evaluated locations on the substrate attained equilibrium for a period of time. As the simulation progressed, equilibrium was broken as heat loss was larger than the heat input, which resulted in a temperature decrease. This phenomenon has been observed in both experimental and

simulation data. Based on this validated model, the temperature history of the first track's middle point from the first, ninth, and 18th layers were predicted and plotted in Figure 3b, which shows the peak temperature is around 3600 K and close to the evaporation temperature of titanium. The layer heat source method validation results are shown in Figure 3c, where the same trend is captured after about 150 seconds, meaning the simulation and experimental data are well matched. The temperature difference at about 150 seconds also comes from the difference in simulation and experimental loading methods. The predicted middle point peak temperature from the first track of the first, ninth, and 18th layers is close to 4200 K using the layer heat source model and exceeds the evaporation temperature of titanium. The peak temperature overestimation comes from the lack of cooling time between each track and layer compared to the real experiments.

Comparing these two methods, the track-heat-source method has a better resolution than the layer-heat-source method, where the former can capture more thermal details better than the latter method. However, compared to the conventional method which applies the heat source spot by spot, both methods have a lower resolution.

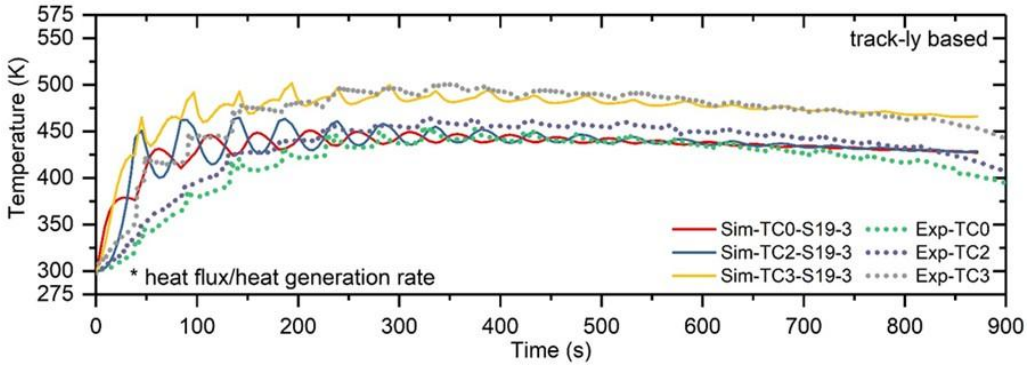

(a) temperature comparison with track heat source method

Figure 3. Model validation results

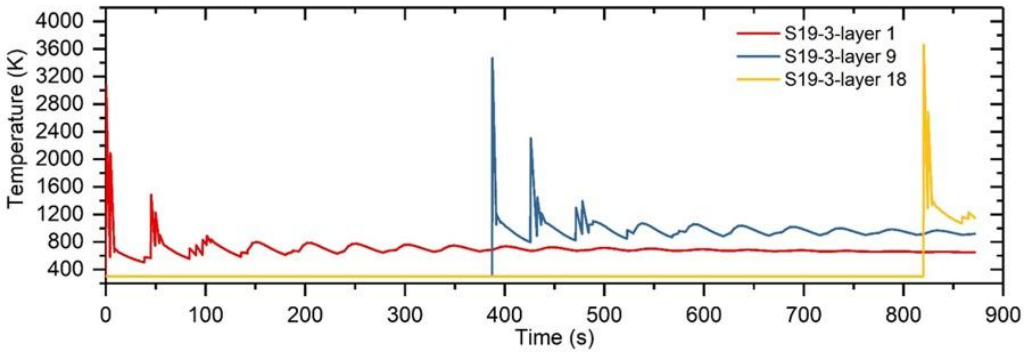

(b) prediction of temperature at first, ninth, and 18th layers with track heat source method

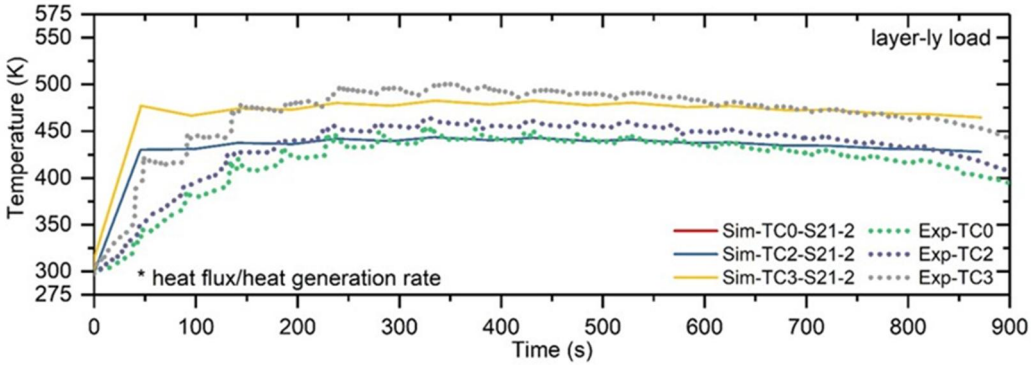

(c) temperature comparison with layer heat source method

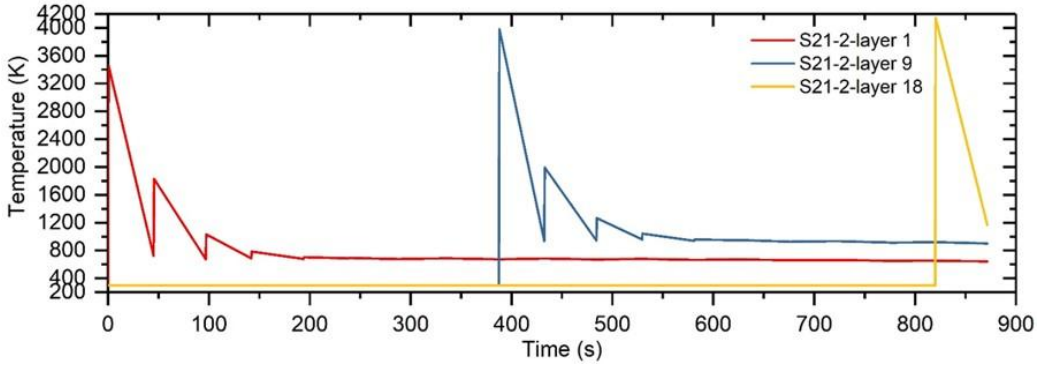

(d) prediction of temperature at first, ninth, and 18th layers with layer heat source method

Figure 3. Model validation results (cont.)

Considering the computational time, the track-heat-source method took about 55 minutes and the layer-heat-source method took about 5 minutes on a computer with an AMD Phenom™ II X6 1090T Processor 3.2 GHz and 16.0 GB RAM hardware. The

rougher the prediction model implemented, the less computational time is needed and sacrifices accuracy of the results.

5. CONCLUSIONS

To conclude, the current work extends the modeling method for fast temperature prediction in large-scale part fabrication using the LMD process. The following are the salient conclusions in the paper:

1. Track- and layer-heat-source methods have the capability for fast temperature prediction in the LMD process.
2. Deposit peak temperature was overestimated in both methods and came from sacrificing modeling details for the computational time-saving purpose.
3. The track-heat-source method has a higher resolution than the layer-heat-source method, but is relatively slower, taking about 11 times longer computational time.

ACKNOWLEDGMENTS

This project was supported by The Boeing Company through the Center for Aerospace Manufacturing Technologies (CAMT), National Science Foundation Grants #CMMI-1547042 and CMMI-1625736, and the Intelligent Systems Center (ISC) at Missouri S&T. Their financial support is greatly appreciated.

REFERENCES

[1] Costa, L., A. M. Deus, T. Reti, and R. Vilar. "Simulation of layer overlap tempering in steel parts produced by laser cladding." Proceedings of the RPD (2002).

[2] Costa, L., R. Vilar, T. Reti, and A. M. Deus. "Rapid tooling by laser powder deposition: process simulation using finite element analysis." Acta Materialia 53, no. 14 (2005): 3987-3999..

[3] Wang, Liang, and Sergio Felicelli. "Process modeling in laser deposition of multilayer SS410 steel." Journal of Manufacturing Science and Engineering 129, no. 6 (2007): 1028-1034.

[4] Crespo, António, and Rui Vilar. "Finite element analysis of the rapid manufacturing of Ti–6Al–4V parts by laser powder deposition." Scripta Materialia 63, no. 1 (2010): 140-143.

[5] Yan, Lei, Yunlu Zhang, and Frank Liou. "A conceptual design of residual stress reduction with multiple shape laser beams in direct laser deposition." Finite Elements in Analysis and Design 144 (2018): 30-37.

[6] Simulia, D. A. S. S. A. U. L. T. "ABAQUS 6.11 analysis user's manual." Abaqus 6 (2011): 22-2.

[7] Yan, Lei, Wei Li, Xueyang Chen, Yunlu Zhang, Joe Newkirk, Frank Liou, and David Dietrich. "Simulation of Cooling Rate Effects on Ti–48Al–2Cr–2Nb Crack Formation in Direct Laser Deposition." Jom 69, no. 3 (2017): 586-591.

[8] Toyserkani, Ehsan, Amir Khajepour, and Steve Corbin. "3-D finite element modeling of laser cladding by powder injection: effects of laser pulse shaping on the process." Optics and lasers in engineering 41, no. 6 (2004): 849-867.

[9] Mills, Kenneth C. Recommended values of thermophysical properties for selected commercial alloys. Woodhead Publishing, 2002.

[10] Heigel, J. C., P. Michaleris, and E. W. Reutzel. "Thermo-mechanical model development and validation of directed energy deposition additive manufacturing of Ti–6Al–4V." Additive manufacturing 5 (2015): 9-19.

[11] Chen, S.Y.; Yang, X.; Dahmen, K.A.; Liaw, P.K.; Zhang, Y. Microstructures and Crackling Noise of Al_xNbTiMoV High Entropy Alloys. *Entropy* **2014**, *16*, 870–884.

SECTION

2. CONCLUSION

Since the HAM process expands the feasibility of the LMD process, it has more abilities in large-scale complex high-performance metal parts development, such as enabling net shape parts fabrication, inner features machining, in-process quality inspection, and speed-up production, while also covering new parts fabrication, existing parts modification, and repair. Thus, it is essential to investigate and correlate processes with outcomes of the HAM process to benefit better understanding and further optimization of the process.

A new methodology was developed for understanding of the impact of processing parameters relevant to the HAM process on microstructures, Vickers hardness, and tensile testing of Ti-6Al-4V fabricated parts. The DOE approach was introduced to explore significant factors of the YS of the final component, where laser energy density, band height, powder feed rate, and preheat conditions were selected as inputs and the YS was set to response. Microstructure characterization and Vickers hardness evaluation within the deposits were conducted for a thorough understanding of the effects of processing parameters on the microstructure size and morphologies and Vickers hardness distribution. A regression model was obtained based on the ANOVA test results to provide guidelines for process stability control and production improvement by setting a different tolerance for process inputs control.

Cutting fluid is essential in Ti-6Al-4V component fabrication with the HAM process, so an investigation of coolant residue removal was conducted. Feasible methods for both oil-based and water-based coolant cleaning in the HAM process for Ti-6Al-4V parts have been obtained. Laser heating and compressed air followed by laser heating can effectively clean oil-based and water-based coolant residue without sacrificing tensile properties. Those innovative methods rely on hardware that is already embedded in the HAM systems, which ensures both build quality and production efficiency.

Narrowing down the process window is critical for cost and time efficiency improvement in the HAM process. The FEA method provides a good option for realizing those goals. To solve the intrinsic issue of low time efficiency in conventional FEA methods of simulating large-scale parts fabrication via the HAM process, two innovative FEA models, track- and layer-heat-source methods were proposed that have the capability of fast temperature prediction in the HAM process. The track-heat-source method has superior in the differentiate resolution of temperature results, but sacrifices computational time, taking about eleven times longer than the layer-heat-source method.

The overall outcomes of this dissertation addressed several key issues that challenge the application of the HAM process. The dissertation provides a systematic approach for developing a build strategy in the HAM process. In addition, the coolant residue removal method guarantees the component's quality and speeds up production efficiency. Moreover, the track- and layer-heat-source methods provide new thoughts in the modeling of large-scale parts fabrication via the LMD or HAM process and benefit the further process improvements.

BIBLIOGRAPHY

[1] Choi, Doo-Sun, S. H. Lee, B. S. Shin, K. H. Whang, Y. A. Song, S. H. Park, and H. S. Jee. "Development of a direct metal freeform fabrication technique using CO2 laser welding and milling technology," Journal of Materials Processing Technology 113, no. 1-3 (2001): 273-279.

[2] Hur, Junghoon, Kunwoo Lee, and Jongwon Kim. "Hybrid rapid prototyping system using machining and deposition," Computer-Aided Design 34, no. 10 (2002): 741-754.

[3] Akula, Sreenathbabu, and K. P. Karunakaran. "Hybrid adaptive layer manufacturing: An Intelligent art of direct metal rapid tooling process," Robotics and Computer-Integrated Manufacturing 22, no. 2 (2006): 113-123.

[4] Bordin, A., S. Sartori, S. Bruschi, and A. Ghiotti. "Experimental investigation on the feasibility of dry and cryogenic machining as sustainable strategies when turning Ti6Al4V produced by Additive Manufacturing," Journal of cleaner production 142 (2017): 4142-4151.

[5] Pramanik, Alokesh, and Guy Littlefair. "Machining of titanium alloy (Ti-6Al-4V)—theory to application," Machining science and technology 19, no. 1 (2015): 1-49.

[6] Pramanik, Alokesh. "Problems and solutions in machining of titanium alloys," The International Journal of Advanced Manufacturing Technology 70, no. 5-8 (2014): 919-928.

[7] Costa, L., A. M. Deus, T. Reti, and R. Vilar. "Simulation of layer overlap tempering in steel parts produced by laser cladding." Proceedings of the RPD (2002).

[8] Costa, L., R. Vilar, T. Reti, and A. M. Deus. "Rapid tooling by laser powder deposition: process simulation using finite element analysis." Acta Materialia 53, no. 14 (2005): 3987-3999..

[9] Wang, Liang, and Sergio Felicelli. "Process modeling in laser deposition of multilayer SS410 steel." Journal of Manufacturing Science and Engineering 129, no. 6 (2007): 1028-1034.

[10] Crespo, António, and Rui Vilar. "Finite element analysis of the rapid manufacturing of Ti–6Al–4V parts by laser powder deposition." Scripta Materialia 63, no. 1 (2010): 140-143.

[11] Yan, Lei, Yunlu Zhang, and Frank Liou. "A conceptual design of residual stress reduction with multiple shape laser beams in direct laser deposition." Finite Elements in Analysis and Design 144 (2018): 30-37.

VITA

Lei Yan was born in Hongze City, Jiangsu province, China. He received his Bachelor of Science degree in Manufacturing Engineering of Aerospace in June 2009 from Nanjing University of Aeronautics and Astronautics, Nanjing, Jiangsu, China. In June 2012, he received his Master of Science degree in Precision Instruments and Machinery from Chinese Academy of Sciences, Nanjing, Jiangsu, China. From July 2012 to July 2014, he worked as a product development engineer at Caterpillar Research and Development Center, Wuxi, Jiangsu, China. In May 2019, he received his Doctor of Philosophy in Mechanical Engineering from Missouri University of Science and Technology, Rolla, Missouri, USA. His research focused on metal additive manufacturing, hybrid additive manufacturing, and finite element analysis of metal additive manufacturing processes. During his Ph.D. study, he won the best paper award at the 26th and 27th Annual International Solid Freeform Fabrication Symposium. He authored and co-authored fourteen journal papers and seven conference papers in the metal additive manufacturing areas.